

# Exploring autophagy-related prognostic genes of Alzheimer's disease based on pathway crosstalk analysis

Fang Qian<sup>#</sup>, Wei Kong<sup>\*\*</sup>, Shuaiqun Wang

## ABSTRACT

Recent studies have shown that different signaling pathways are involved in the pathogenesis of Alzheimer's disease (AD), with complex molecular connections existing between these pathways. Autophagy is crucial for the degradation and production of pathogenic proteins in AD, and it shows link with other AD-related pathways. However, the current methods for identifying potential therapeutic targets for AD are primarily based on single-gene analysis or a single signal pathway, both of which are somewhat limited. Finding other methods are necessary for providing novel underlying AD therapeutic targets. Therefore, given the central role of autophagy in AD and its interplay with its pathways, we aimed to identify prognostic genes related to autophagy within and between these pathways based on pathway crosstalk analysis. The method of pathway analysis based on global influence was applied to find the feature mRNAs involved in the crosstalk between autophagy and other AD-related pathways. Subsequently, the weighted gene coexpression network analysis was used to construct a coexpression module of feature mRNAs and differential long non-coding RNAs. Finally, based on two autophagy-related crosstalk genes (CD40 and SMAD7), we constructed a prognosis model by multivariate Cox regression, which could predict the overall survival of AD patients with medium-to-high accuracy. In conclusion, we provided an effective method for extracting autophagy-related significant genes based on pathway crosstalk in AD. We found the biomarkers valuable to the AD prognosis, which may also play an essential role in the development and treatment of AD.

**KEYWORDS:** Alzheimer's disease; autophagy; prognostic signature; pathway crosstalk; weighted gene coexpression network analysis; pathway analysis method based on global influence

## INTRODUCTION

Alzheimer's disease (AD) is one of the common forms of dementia, and its typical pathological features are the presence of amyloid (A $\beta$ ) deposition, hyperphosphorylated tau protein aggregation, and neurofibrillary tangles in the brain [1]. Although the pathological relevance is known, the exact pathogenesis of AD is still poorly understood. Research in recent years has discovered and explained many signal pathways related to AD, among which the key role of the autophagy pathway in AD is becoming more and more prominent [2]. Autophagy is a crucial regulator of the A $\beta$  and tau proteins production. A $\beta$  and tau proteins can induce autophagy as well to promote its clearance through the mTOR pathway or

independently [3,4]. Many studies have shown that normal autophagy protects neurons, but dysfunctional autophagy may increase the deterioration of neurons in AD [5,6]. In addition, there are interactions between autophagy and other related signaling pathways, which provide new possibilities for exploring the pathogenesis and therapeutic targets of AD.

With the innovation of RNA sequencing technology and bioinformatics analysis, the identification of hub genes and functional pathways in AD has developed rapidly [7]. In addition to mRNA, long non-coding RNA (lncRNA) has also been found to be involved in the pathological progress of AD, including the induction of autophagy to promote the clearance of A $\beta$  or tau protein, the inhibition of neuroinflammation, and other biological processes [8,9]. Studying the molecular mechanism of these RNAs and their interaction with autophagy will provide promising AD diagnosis and treatment methods [10,11].

Although these RNAs play a crucial role in AD, most of the current methods for their excavation are based on bioinformatics analysis and competition with endogenous RNA hypotheses, which may ignore their interconnection with autophagy or crosstalk between pathways. In excavating disease-causing genes, the above methods may fail to identify more meaningful molecular targets. Therefore, it is necessary to find new effective strategies.

With the accumulation of high-throughput genome-wide expression data, researchers can systematically study

Department of College of Information Engineering, Shanghai Maritime University, Shanghai, China

\*Corresponding author: Wei Kong, College of Information Engineering, Shanghai Maritime University, 1550 Haigang Ave, Shanghai, 201306, China. E-mail: weikong@shmtu.edu.cn

<sup>#</sup>These authors equally contributed

DOI: <https://doi.org/10.17305/bjbms.2021.7019>

Submitted: 5 February 2022/Accepted: 26 March 2022/Published online: 2 April 2022

Conflicts of interest: The authors declare no conflicts of interest.

Funding: The research was conducted with support from the Natural Science Foundation of Shanghai (No.18ZR1417200) and the National Natural Science Foundation of China (No.61803257).



©The Author(s) (2021). This work is licensed under a Creative Commons Attribution 4.0 International License

the functional relationship of single or several genes in diseases [12]. It is well known that genes do not function in isolation but work together within various metabolic, regulatory and signaling pathways. Furthermore, increasing evidence shows that pathway-based methods are generally superior to gene-based counterparts [13].

Methods based on pathway analysis can explain complex biological processes and biological significance. AD is a multifactorial disease involving multiple cell signaling pathways, so crosstalk within and between pathways exists. Because the number and combinations of signals are limited, crosstalk between pathways can create novel input/output combinations. Having more input/output combinations increases the possible ways of the signaling information flow within the cell, allowing more diverse phenotypes. Thus, genes generated by crosstalk play an essential role in the generation and development of disease [2,14,15].

Several recent techniques have used path topology information to identify dysfunctional paths. The pathway analysis based on the global influence (PAGI) algorithm utilizes gene networks [16], looking for dysregulated pathways in diseases by considering the internal effects of pathways and crosstalk between pathways, which provides the possibility for the AD exploration.

Studies have shown that lncRNA can directly mediate crosstalk in pathways by cooperating with coding genes that play an important role in diseases [17]. In addition, lncRNAs and mRNAs can compete with each other through miRNAs response elements to regulate AD progress [18]. Based on the interaction of autophagy with the RNA mentioned above and other signal pathways in AD, it is believed to be a novel idea to investigate the role of autophagy-related genes in AD and their pathogenic mechanisms in diseases from the perspective of pathway crosstalk.

Our research introduced a novel method to identify prognostic genes related to autophagy in AD. First, the PAGI pathway analysis algorithm was applied to gene expression data in order to obtain pathways and crosstalk genes associated with AD. Second, the WGCNA algorithm was used to select significant genes with coexpression relationships, and genes in the same expression module may have similar biological functions [19].

Finally, the survival analysis was applied to significant genes, and the prognostic genes of AD were extracted. Results showed that based on PAGI, more than 36 autophagy-related pathways dysregulated and crosstalk with each other in AD. Furthermore, 103 lncRNAs and 650 mRNAs related to autophagy with coexpression relationships were identified using WGCNA analysis. Next, CD40 and SMAD7 were identified as prognostic genes of AD, which was also verified in the external AD dataset. Finally, we performed prognostic survival

analysis and differential expression analysis on the other AD data to verify the prognostic genes. The experimental results confirmed our conclusions.

## MATERIALS AND METHODS

### Data source

The data used in this study was obtained from subjects of the Religious Order Study (ROS) or the Rush Memory and Aging Project (MAP), which are two prospective clinical-pathological cohort studies of aging and dementia. The two studies (collectively referred to as ROSMAP) share clinical and neuropathological standards, allowing joint data analysis [20,21]. Moreover, the ROSMAP study is stored in the AD Knowledge Portal (<https://adknowledgeportal.synapse.org/>).

The gene expression profile (syn8691134) and clinical information needed for this research were obtained from the AD Knowledge Portal database (the raw count data can be obtained online at <https://www.synapse.org/#!Synapse:syn8691134>, the filtered raw count data can be obtained online at <https://www.synapse.org/#!Synapse:syn8456637>, and the clinical data were downloaded online at <https://www.synapse.org/#!Synapse:syn3191087>). According to clinical information, we screened 155 AD samples and 86 normal samples as the data for this study. The validation dataset (syn4009614) was obtained from the AMP-AD Knowledge Portal database (the normalized data can be obtained online at <https://www.synapse.org/#!Synapse:syn4009614>).

We downloaded the autophagy gene file from the Human Autophagy Database (<http://www.autophagy.lu/>) and HAMdb (<http://hamdb.scbdd.com/>) for the annotation of autophagy genes on the pathway. The experimental flowchart of this paper is shown in the Figure 1, and we will discuss each part in detail later.

### Data preprocessing

According to the human genome assembly GRCh38, the ensemble ID of the raw count data was switched to the gene symbol. According to the gene type annotation, the genes in the raw data were divided into 19,677 mRNAs and 14,259 lncRNAs. We only kept the highly expressed mRNA (obtained from filtered count data syn8456637, deleted genes whose count is <1 CPM in at least 50% of the samples, and deleted genes whose length and GC content are missing). Then, we performed TPM standardization and normalization on the filtered mRNA expression profile and used the SVA package to eliminate batch effects (sequencing batch of samples, nine batches in total) in the standardized data.

The R package "DESeq2" was used to identify differentially expressed lncRNAs (DELncRNAs) [22]. First, we used

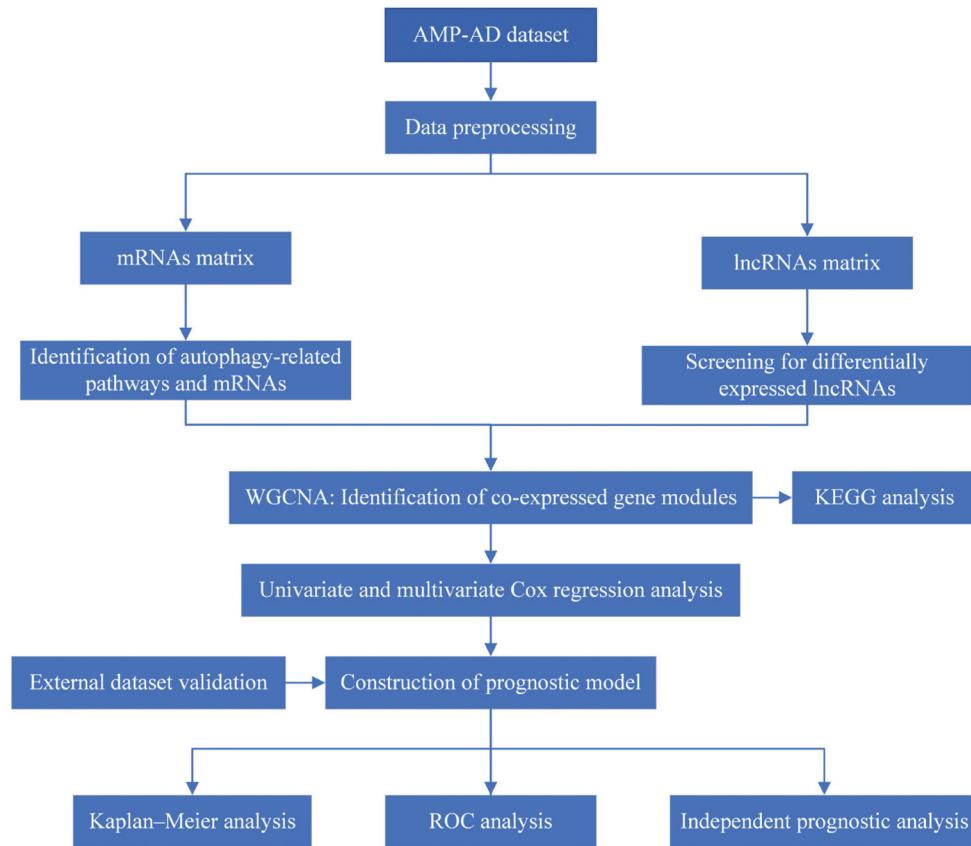


**FIGURE 1.** Framework of the experiment.

the DESeqDataSetFromMatrix function to convert the count matrix into a DESeqDataSet (DDS) object. The formula of the design parameter of DESeqDataSetFromMatrix function is as follows: design=~batch+group, where batch represents the sequencing batch information of the sample (batch value is from 0 to 8), group is the grouping information of the sample (the samples were divided into diseased group and normal group). Then, we used the DESeq function to normalize (by calculating the size factor of each column of samples in the count matrix) DDS and analyze the differential expression of lncRNAs in normal and diseased samples. The selected criteria for screening differentially expressed lncRNAs was taking  $p < 0.05$  into consideration, and a log2FC range of  $-0.5-0.5$  was rejected.

**PAGI**

The PAGI algorithm is a pathway analysis method based on global influence, which identifies dysregulated pathways by considering both within-pathway effects and crosstalk between pathways. We used the PAGI algorithm to identify dysregulated pathways in AD. Principle of the PAGI algorithm is as follows:

First, constructing the global gene-gene network. Based on the structural information and genetic relationship of each pathway in KEGG, the “iSubpathwayMiner” system was used to construct a global gene network that reflected the relationship between and within a pathway [23,24].

Second, calculating the global dysregulated score (GDS). GDS was used to assess the degree to which genes are affected by the internal effects of pathways and crosstalk between pathways. The Random Walk with Restart (RWR) algorithm captures global relationships within a network and can calculate the node’s proximity to a set of source nodes [25]. In the application process, the two-sample (diseased and normal samples) t-test was performed to evaluate the extent of differential expression (t-score). All genes represented in the gene expression profile were mapped to the global network as source nodes. The RWR algorithm was modified by combining the t-score and the global network topology to calculate GDS and reflect the global influence of the gene on the source nodes. The revised algorithm formula is as follows:

$$p^{t+1} = (1-r)Mp^t + rp^0 \tag{1}$$

Where, M is the column-normalized adjacency matrix of the global network graph G,  $p^t = (p_1^t, p_2^t, \dots, p_n^t)$  is the node vector at time t, and its  $i^{th}$  element  $p_i^t$  represents the probability of being at node i at time t, and n represents the number of all nodes (genes) in G. r is the restart probability, which controls the degree to which the random traverser returns to the source node in each iteration.

The initial probability  $p^0 = (p_1^0, p_2^0, \dots, p_n^0)$  is normalized to the unit vector  $p_i^0 = |t-score|_i / \sum |t-score|_i$ . The higher the  $p_i^0$  of gene i, the greater the degree of disturbance to other genes.  $p^t$  can reach a stable state  $p^*$  after

multiple iterations, it was used to measure the GDS of genes. The GDS of gene  $i$  was assigned by the normalized  $p_i^\infty$  as:  $GDS_i = (p_i^\infty - \min(p^\infty)) / (\max(p^\infty) - \min(p^\infty))$ . Through this method, the GDS of each gene in the global network can be obtained.

Third, identification of dysregulated pathways. The gene list  $L = \{g_1, g_2, g_3, \dots, g_n\}$  consists of all genes in the expression profile sorted according to  $t_j^{1+GDS_j}$ ,  $t_j$  represents |t-score| of gene  $j$ , and  $GDS_j$  represents GDS of gene  $j$ . The dysfunction score of  $p$  path is calculated based on the information of its gene mapping in the  $L$  path and is calculated by cumulative distribution functions (CDFs). The CDFs of  $Inp$  (genes in  $P$ ) and  $Notp$  (genes in  $L$ , not in  $P$ ) are used to evaluate the fraction of genes in  $p$  weighted by their correlation ( $t_j^{1+GDS_j}$ ), and the fraction of genes not in  $P$  presents up to a given position  $i$  in  $L$ . The formula is as follows:

$$CDF_{Inp}(i) = \sum_{\substack{g_i \in P \\ j \leq i}} \frac{t_j^{1+GDS_j}}{N_R} \tag{2}$$

and

$$CDF_{Notp}(i) = \sum_{\substack{g_i \notin P \\ j \leq i}} \frac{1}{N_{NotP}} \tag{3}$$

Where,  $N_R = \sum_{g_i \in P} t_j^{1+GDS_j}$ ;  $N_{NotP}$  represents the number of genes in  $L$  not in  $P$ . With the position  $I$  walking down the list  $L$ , the formula for calculating the dysfunction score of path  $P$  is as follows:

$$S_p = \max_{i \in L} \{CDF_{Inp}(i) - CDF_{Notp}(i)\} \tag{4}$$

Finally, the significantly dysregulated pathways in AD obtained according to the false discovery rate ( $FDR < 0.01$ ) were used as candidate pathways. According to the autophagy gene annotation results of each candidate pathway and the literature review, the pathways that interact with autophagy were selected as the feature pathways, and the mRNAs in the feature pathway were used as the feature mRNAs.

### Construction of coexpression gene modules based on WGCNA analysis

The R package "WGCNA" was used to identify DElncRNAs and feature mRNAs with coexpression relationship. Therefore, the feature mRNAs and DElncRNAs served as the input of WGCNA. First, the absolute value of the Pearson correlation coefficient between genes was used to construct the correlation matrix ( $S_{ij}$ ,  $i$  and  $j$  indicate the  $i^{th}$  and  $j^{th}$  gene). The threshold of the fitting index was set to 0.85 ( $R^2 > 0.85$ ) to fit with the scale-free network. When the fitting index reached 0.85, the  $\beta$  value (soft threshold) that maximized the average connectivity was selected to perform a power-law operation to convert the correlation matrix into an adjacency matrix ( $a_{ij}$ ,  $a_{ij} = |S_{ij}|^\beta$ ) [26].

Then, the pickSoftThreshold function was used to calculate the corresponding and average connectivity for different  $\beta$  values (the  $\beta$  values were set between 1 and 20). Next, we transformed the adjacency matrix into a topological overlap matrix. We used the DynamicTreeCut algorithm to construct the average linkage hierarchical clustering dendrogram [27]. Finally, we calculated the module Eigengenes, hierarchically clustered the modules, and merged similar modules [28].

### Functional enrichment analysis

KEGG analysis was used to explore the biological functions of genes on coexpressed modules [29]. The filter condition of the enrichment pathway was that  $p$ -value and the adjusted  $p$ -value ( $q$ -value) were both less than 0.05. Finally, according to the results of KEGG enrichment, the gene modules needed in this study were obtained, and the genes in the modules were used as AD significant genes.

### Cox proportional hazards regression analysis

To obtain significant genes related to the prognosis of AD, we used the R package "survival" to perform univariate and multivariate Cox regression analysis on the AD candidate biomarkers (genes in the turquoise module). To verify the validity of the prediction model, we used syn8691134 as the training dataset, and syn8691134 and syn4009614 datasets were combined as the testing dataset. First, we extracted the expression data of genes belonging to the turquoise module in the training dataset and the testing dataset, and the expression data of their overlapping genes were used as the input of univariate Cox regression analysis.

Then, univariate Cox regression analysis was used to identify genes significantly related to the overall survival (OS) of patients with AD. The criterion for screening genes related to the OS of patients with AD is that  $p < 0.01$  was considered. Next, we performed multivariate Cox regression analysis on the genes screened by univariate Cox regression analysis and constructed a prognostic-related model of AD. We used the stepwise selection of variables based on the lowest Akaike information criterion (AIC) to optimize the prognostic-related model of AD. We calculated the risk score of each patient, which can be used to divide AD patients into a high-risk group and a low-risk group. The formula is as follows:

$$Risk\ Score = \sum_{k=1}^n coef(k) * x(k) \tag{5}$$

Where,  $coef(k)$  represents the Cox regression coefficient,  $x(k)$  represents the expressive value of each genes, and  $n$  represents the number of genes.

Finally, the Kaplan–Meier (KM) curve and forest plot of multivariate Cox regression analysis were generated by R package "survival." The KM curve was used to judge whether

it exists a difference in survival between the high-risk and the low-risk groups. The forest plot was used to judge whether the risk score is an independent prognostic factor affecting OS. Then time-dependent receiver operating characteristic (ROC) curve and the multi-index ROC curve were used to evaluate the accuracy of the prognostic-related model by R package "timeROC."

## Statistical analysis

According to the test condition, Wilcoxon test was used to perform statistical comparisons between two groups of data, and  $p < 0.05$  was used to indicate statistical significance. The GSE118553 and GSE5281 AD dataset were obtained from the GEO platform (<https://www.ncbi.nlm.nih.gov/geo/>).

## RESULTS

### Data preprocessing results and DElncRNAs

After quality control and TPM standardization of mRNAs data, 13,556 mRNAs were obtained. Then, the standardized data were adjusted in batches (nine batches in total) through the combat function of the SVA package, and the adjusted data were reserved as the input of the PAGA algorithm.

To identify differentially expressed lncRNAs, we used the DESeq2 package to standardize the gene expression profile of lncRNAs and analyze differential expression. The lncRNAs with  $p < 0.05$  and  $|\log_2FC| > 0.5$  were extracted as statistically significant differential genes. Finally, 180 differentially expressed lncRNAs were obtained, of which 75 were upregulated and 105 were downregulated. The top 30 differential genes (15 down and 15 up) are shown in the Supplemental Table 1.

### Exploring autophagy-related pathways based on PAGA

To explore autophagy-related biomarkers in AD from the perspective of pathway crosstalk, we applied the mRNA expression profile of AD to the PAGA algorithm. According to the FDR value  $< 0.01$ , 94 pathways related to AD were screened

out. Then, by consulting the literature and annotating the autophagy genes on each pathway, 36 autophagy-related pathways and crosstalk genes required for this study were screened out. A total of 1436 crosstalk genes (feature mRNAs) were included in the 36 pathways, which were one of the input data of the WGCNA algorithm.

Ten out of the 36 pathways were confirmed to be related to autophagy in AD and are shown in Table 1, and information about the remaining pathways is shown in Supplemental Tables 2 and 3. The 10 pathways and their crosstalk genes (GDS score ranks top 20 in the pathway) were displayed in a pathways-gene network in Figure 2. From Figure 2, it can be seen that genes in hsa047229 (Neurotrophin signaling pathway) and hsa04310 (Wnt signaling pathway) pathways had higher GDS scores, while genes on hsa04141 (Protein processing in endoplasmic reticulum) pathways had lower GDS scores.

In addition, based on the KEGG database (<https://www.kegg.jp/>), we explored other diseases associated with autophagy-related crosstalk genes in AD (Supplemental Table 4) and mapped related genes in AD pathways (Supplemental Figure 1). These genes, which are related to other diseases, may affect the progression of AD by participating in signaling pathways such as the calcium signaling pathway, insulin signaling pathway and calcium signaling pathway in AD.

In Table 1, the first column is the pathway name based on PAGA algorithm screening, the second column is the pathway ID, and the third column "Size" indicates the number of genes contained in the pathway, the fourth column "Pathway Score" is the score after the pathway passes the PAGA algorithm, the fifth column "Gene%" is the percentage in the gene list before running enrichment peak, and the sixth column "Signal" indicates the intensity of the enrichment signal, and the seventh column is the number of autophagy genes included in the pathway.

It can be seen from Table 1 that the scores of these 10 pathways were all higher than 0.4, and the pathway score of AD (hsa05010) pathway was 0.42487, which directly proved the effectiveness of the pathway selection through PAGA. Furthermore, the pathway score of the mTOR signaling

**TABLE 1.** Ten pathways related to autophagy identified by the PAGA

Pathway name	Pathway ID	Size	Pathway score	Gene/%	Signal	Autophagy
Protein processing in endoplasmic reticulum	hsa04141	152	0.44823	0.308	0.359	33
Apoptosis	hsa04210	70	0.44783	0.152	0.231	28
Alzheimer's disease	hsa05010	132	0.42487	0.37	0.357	21
mTOR signaling pathway	hsa04150	46	0.48142	0.15	0.297	23
Insulin signaling pathway	hsa04910	119	0.51274	0.0637	0.262	30
Neurotrophin signaling pathway	hsa04722	114	0.54769	0.144	0.326	32
Endocytosis	hsa04144	174	0.42422	0.192	0.268	35
Type II diabetes mellitus	hsa04930	32	0.5506	0.0875	0.314	8
Wnt signaling pathway	hsa04310	123	0.4932	0.0972	0.252	12
Calcium signaling	hsa04020	133	0.57959	0.167	0.367	8

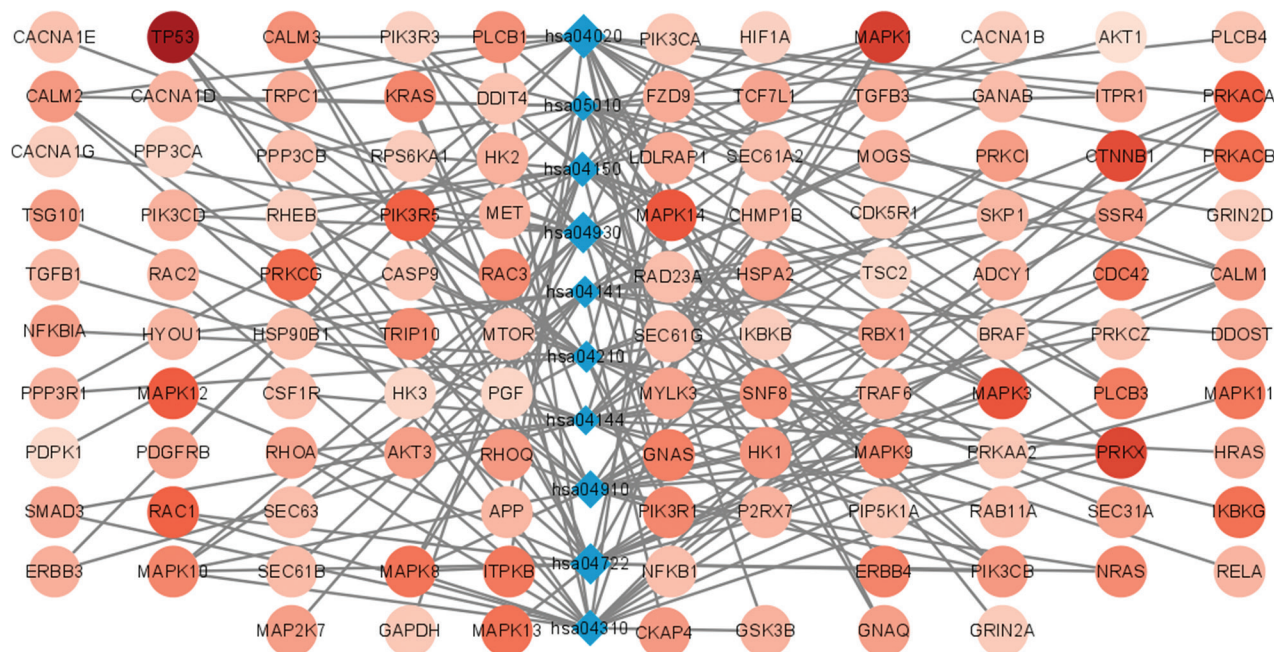


**FIGURE 2.** Network connection diagram of 10 pathways and their crosstalk genes. The blue diamond nodes represent different pathways, and the size of the nodes represents the score of the pathway in PAGA. The circular node connected to the blue diamond node represents the genes included in the pathways. The shade of the color represents the level of the gene's GDS score. The darker the node's color, the higher the GDS score represents the gene. hsa04141: Protein processing in endoplasmic reticulum. hsa04210: Apoptosis. hsa05010: Alzheimer's disease. hsa04150: mTOR signaling pathway. hsa04910: Insulin signaling pathway. hsa04722: Neurotrophin signaling pathway. hsa04144: Endocytosis. hsa04930: Type II diabetes mellitus. hsa04020: Calcium signaling.

pathway (hsa04150) was 0.48142, which is currently one of the most promising targets for autophagy-related AD therapy [3]. Moreover, autophagy genes (489 in total) in the selected pathways all account for a high proportion, which provided a basis for extracting autophagy-related crosstalk genes.

### Analysis of autophagy-related coexpression module

To obtain feature mRNAs (autophagy-related crosstalk genes) and lncRNAs with a coexpression relationship, we used the WGCNA algorithm to construct a coexpression module for it. First, we obtained the count matrix composed of differentially expressed lncRNAs and autophagy-related crosstalk genes.  $\beta=6$  ( $R^2=0.89$ ) was set as the soft-thresholding parameter to construct the scale-free network (Figure 3A). The number of genes in each module was defined as at least 50. Next, seven modules were identified based on DynamicTreeCut algorithm. Finally, based on the module Eigengenes, the height of cut was 0.25 to merge similar modules (Figure 3B). Moreover, six coexpression modules were identified (Figure 3C). The six modules are shown in Table 2. From Table 2, we can see that the number of autophagy genes in the turquoise module is the largest among the six modules.

KEGG pathway enrichment analysis was performed on the genes of each module, and the turquoise module was finally determined as the research object according to the

analysis results. The turquoise module includes 103 lncRNAs and 650 mRNAs. One hundred and one of the 650 mRNAs are located in the AD pathway (369 genes), and 45 are autophagy genes (489 genes), as shown in Figure 4. From Figure 4, the crosstalk genes in the turquoise module overlap more with the genes in autophagy and AD pathway (hsa05010), indicating that the coexpression module we selected has a correlation with AD and autophagy. Pathway enrichment analysis of gene modules was implemented by David (<https://david.ncifcrf.gov/>) [30].

The pathway enrichment results of the turquoise module are shown in Figure 5. David obtained the first 20 pathways with  $p < 0.05$ , including AD pathway, pathways of neurodegeneration-multiple diseases, and PI3K-Akt signaling pathway [31]. The discovery of the above pathways directly proved the significance of the turquoise module as a research object. Moreover, the genes on the turquoise module are also involved in MAPK signaling pathway [32], protein processing in endoplasmic reticulum [33], calcium signaling pathway [34], focal adhesion [35], insulin signaling pathway [36], neurotrophin signaling pathway [37], regulation of actin cytoskeleton [38], endocytosis [39], and Ras signaling pathway [40].

In Table 2, the first row is the name of the six coexpression modules, and each column represents the number of lncRNA, mRNA, and autophagy genes contained in the module.

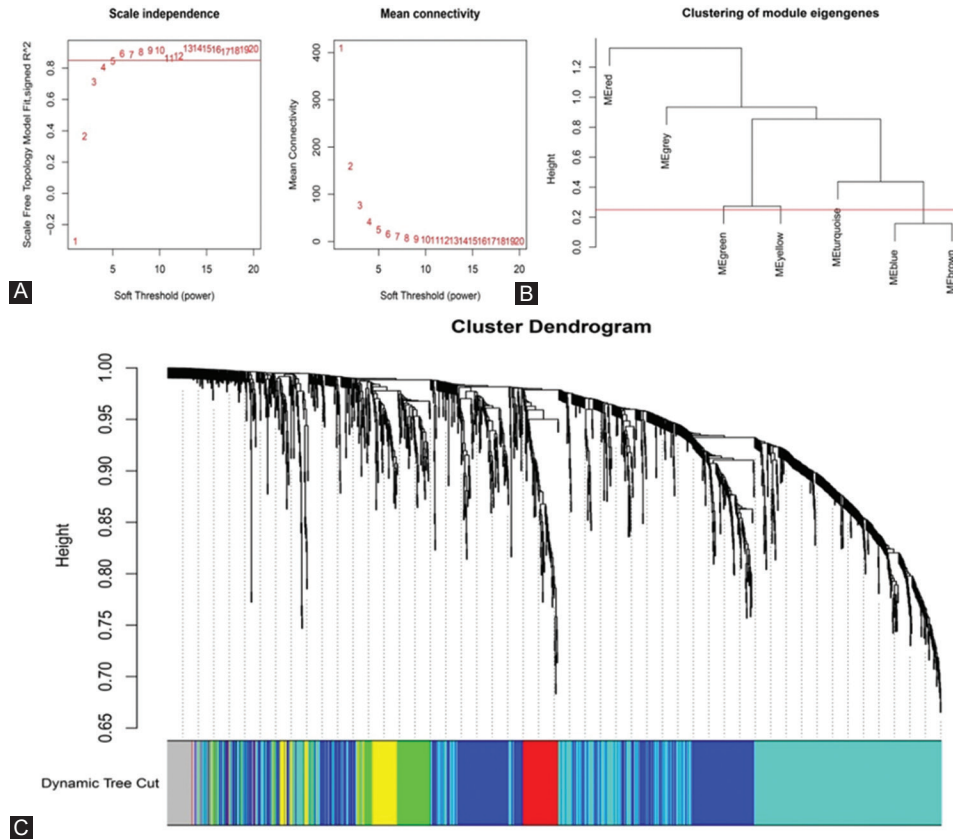


**FIGURE 3.** Network construction of coexpressed genes. (A) Analysis of the scale independence and mean connectivity for various soft-threshold powers; (B) the cluster dendrogram of module Eigengenes; (C) dendrogram clustered based on a dissimilarity measure (1-TOM).

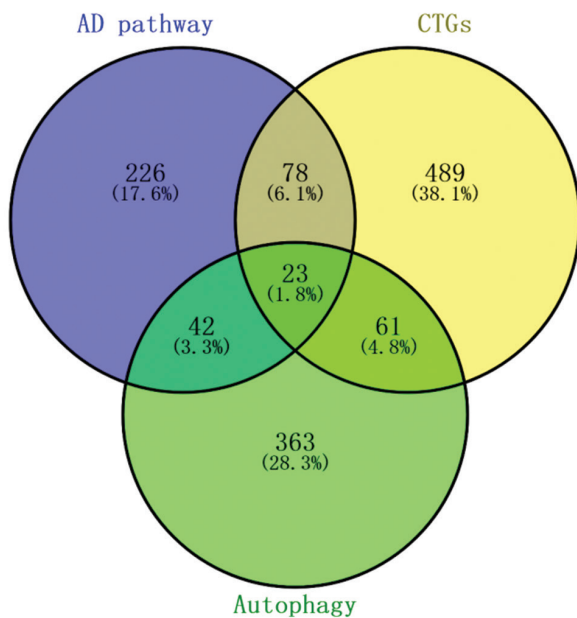


**FIGURE 4.** Venn diagram showing the overlap of crosstalk genes, autophagy-related genes (autophagy), and Alzheimer's disease pathway genes (AD pathway, hsa05010).

### Construction of an autophagy-related prognostic gene model

The clinical data downloaded from the AMP-AD database were sorted and screened. Then, the survival time and clinical

**TABLE 2.** Six coexpressed gene modules obtained by WGCNA

Module	Blue	Green	Gray	Red	Turquoise	Yellow
Number of lncRNAs	16	3	53	4	104	3
Number of mRNAs	470	102	27	82	650	102
Number of autophagy genes	64	19	3	4	84	18

characteristics (braaksc: Braak stage, ceradsc: Assessment of neuritic plaques, and dcfdx\_iv: Clinical cognitive diagnosis summary at last visit) of 82 AD patients in the training dataset and 137 AD patients in the testing dataset were obtained (Supplemental Table 5). Based on the results of WGCNA and KEGG, we selected the genes in the turquoise module (754 genes) for the following analysis. Among the overlapping genes of training dataset and testing dataset, 631 genes belong to the turquoise module. Then, we used the expression data of these 631 genes in training dataset as the input of univariate Cox regression analysis. According to  $p$ -value ( $p < 0.01$ ), we screened 12 genes that were significantly related to the prognosis of AD (Table 3). Subsequently, we performed multivariate Cox analysis on 12 prognostic-related genes obtained from univariate Cox regression analysis. Afterward, according to the lowest AIC value, the prognostic risk model of two genes (CD40 and SMAD7) of the training dataset was constructed. The risk score is expressed as: risk score = (CD40 exp.\* -1.13) + (SMAD7 exp.\* -1.41) (Table 4). Patients with AD in training

dataset and testing dataset were divided into low- and high-risk groups based on the median risk score in the training dataset.

According to the median risk score, 82 AD patients in the training dataset were divided into high-risk (n = 41) and low-risk (n = 41) groups. It can be seen from the KM curve that the OS rate of high-risk patients was significantly lower compared with low-risk patients within 5 years (Figure 6A). Multivariate Cox regression analysis revealed that the risk score of prognostic risk

**TABLE 3.** Twelve autophagy-related crosstalk genes associated with AD overall survival time were obtained from univariate Cox regression analysis

id	HR	HR.95L	HR.95H	p-value
<i>LRP5</i>	0.233636	0.077723	0.702308	0.009618
<i>TLN1</i>	0.259479	0.096078	0.700778	0.007782
<i>CD40</i>	0.172931	0.04894	0.611054	0.006434
<i>PLCG1</i>	0.232832	0.085531	0.633813	0.004339
<i>SMAD7</i>	0.181477	0.066411	0.495911	0.000877
<i>DNM2</i>	0.219818	0.071389	0.676855	0.008287
<i>ARRB1</i>	0.276896	0.111948	0.684888	0.00545
<i>PIK3CD</i>	0.20401	0.062679	0.664023	0.008292
<i>MAP3K3</i>	0.097144	0.020732	0.455191	0.003089
<i>SSH1</i>	0.21241	0.065672	0.687017	0.009688
<i>RAF1</i>	0.174725	0.048116	0.634484	0.008016
<i>RPS6KBI</i>	0.210312	0.067371	0.656535	0.007265

**TABLE 4.** Two autophagy-related prognostic genes were obtained from multivariate Cox regression analysis

id	Coef	HR	HR.95L	HR.95H	p-value
<i>CD40</i>	-1.13112	0.322671	0.086041	1.210083	0.093501
<i>SMAD7</i>	-1.40787	0.244663	0.07868	0.760809	0.015006

model ( $p = 0.002$ ) was an independent prognostic factor affecting the OS of patients with AD in training dataset (Figure 6B). The area under the ROC curve (AUC) was calculated to assess the predictive ability of the model. The 3- and 5-year AUCs were 0.643 and 0.758 (Figure 6C). The multi-index ROC curve showed that the AUC value of the risk score based on the prognostic risk model was greater than 0.7 (AUC = 0.758), which was more significant than other clinical prognostic indicators, such as *braaksc*, *ceradsc*, and *dcfdx\_lv* (Figure 6D).

The results of the Kaplan–Meier analysis showed that patients with high-risk scores had less survival time in the testing datasets ( $p < 0.001$ ) (Figure 7A). The forest plots of the multivariate independent prognostic analysis indicated that the risk score of prognostic risk model ( $p < 0.001$ ) was an independent prognostic factor affecting the OS of AD patients in testing dataset (Figure 7A and B). From time-dependent ROC curve of testing dataset, the 3- and 5-year AUCs were 0.672 and 0.746 (Figure 7C). The multi-index ROC curve showed that the AUC value of the risk score based on the prognostic risk model was  $>0.7$  (AUC = 0.737), which was more significant than other clinical prognostic indicators, such as *braaksc*, *ceradsc*, and *dcfdx\_lv* (Figure 7D). The above results proved the accuracy of the prognostic risk model.

### The expression of CD40 and SMAD7

Finally, we explored the expression of CD40 and SMAD7 in AD and normal brain tissues using GSE5281, GSE118553,

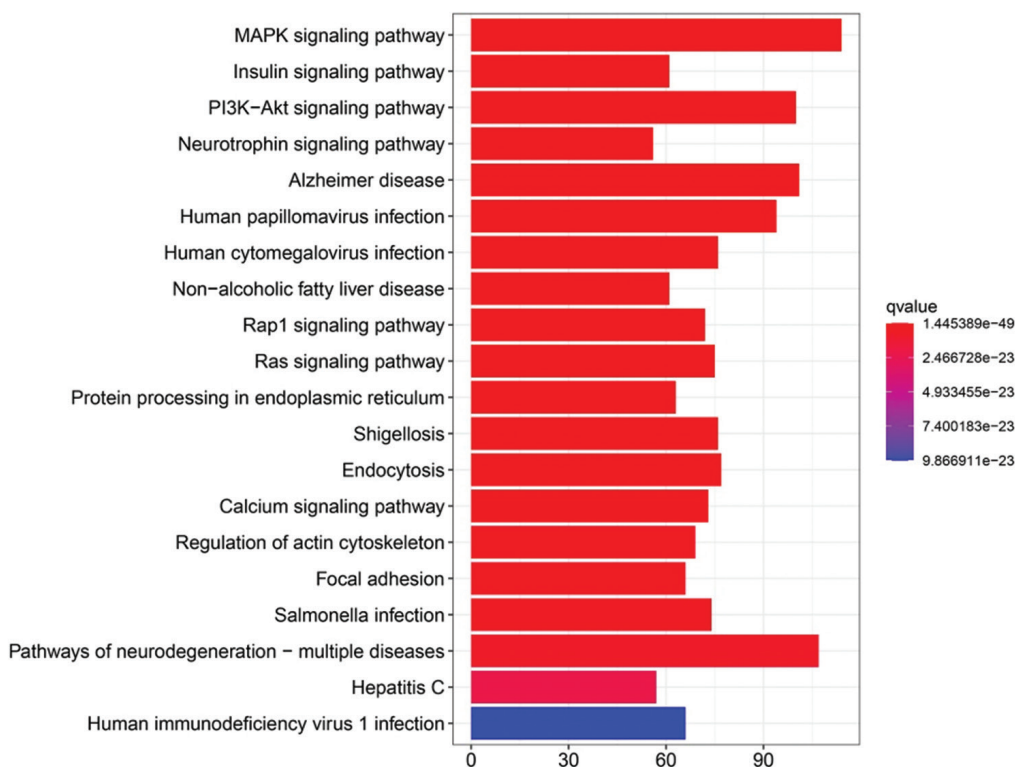


**FIGURE 5.** The results of pathway enrichment. The horizontal axis is the number of genes in the pathway, and the vertical axis is the pathway list. Red to blue indicates the q-value (adjusted p-value).

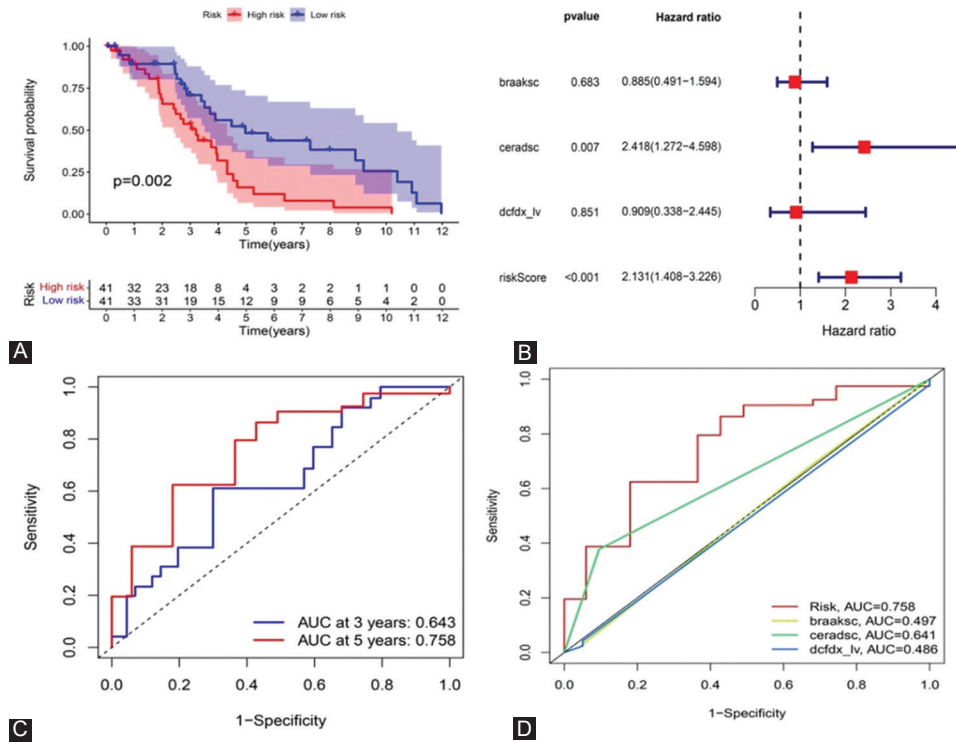


**FIGURE 6.** Prognostic significance analysis of the Alzheimer's disease training dataset. (A) Kaplan–Meier curve to compare OS of high risk with low-risk samples ( $p = 0.002$ ); (B) forest plot of multivariate independent prognostic analysis. The square on the horizontal line shows the hazard ratio (HR), and the horizontal line represents the 95% confidence interval; (C) time-dependent receiver operating characteristic (ROC) curve analysis of the risk score model for predicting 3- and 5-year OS; and (D) multi-index ROC curve. The curve area is used to assess the accuracy of the risk model (model AUC = 0.758).

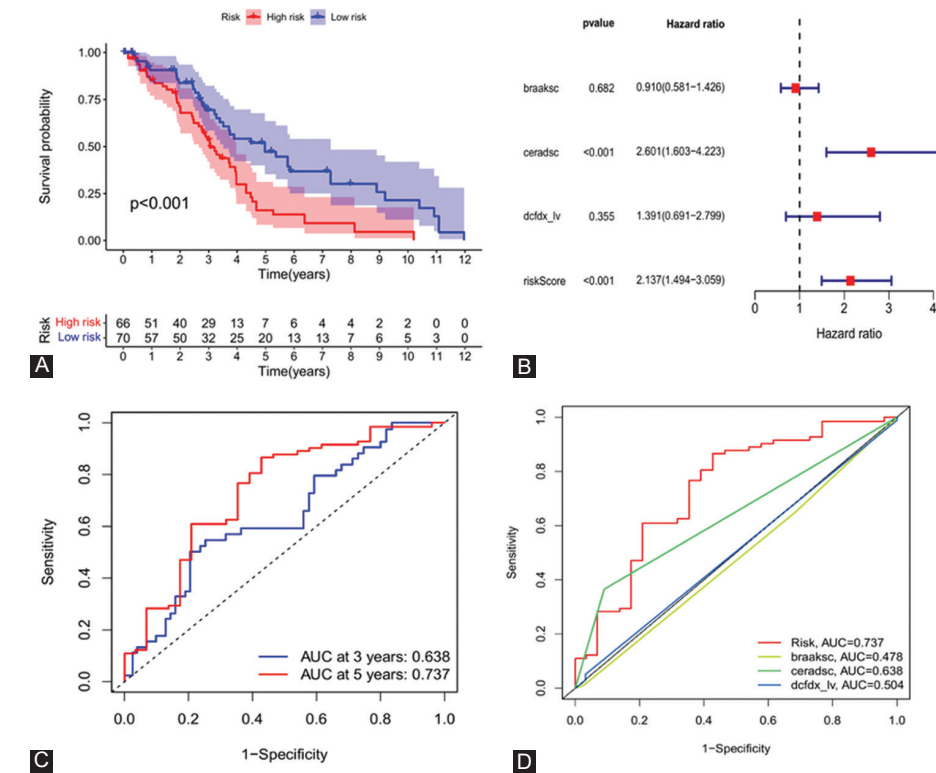


**FIGURE 7.** Prognostic significance analysis of the Alzheimer's disease testing dataset. (A) Kaplan–Meier curve to compare OS of high risk with low-risk samples ( $p < 0.001$ ); (B) forest plot of multivariate independent prognostic analysis. The square on the horizontal line shows the hazard ratio (HR), and the horizontal line represents the 95% confidence interval; (C) time-dependent receiver operating characteristic (ROC) curve analysis of the risk score model for predicting 3- and 5-year OS; and (D) multi-index ROC curve. The curve area is used to assess the accuracy of the risk model (model AUC = 0.737).

and syn4009614. As shown in the following figures below, we observed that CD40 (Figure 8A-C) and SMAD7 (Figure 9A-C) were significantly upregulated in AD.

## DISCUSSION

### Extract autophagy-related pathways based on pathway crosstalk

A variety of signal pathways in AD are involved in the generation and development of disease, and crosstalk is inevitable between these signal pathways. Crosstalk between pathways provides a novel combination of non-linear response dysfunction. Furthermore, genes generated by crosstalk play an essential role in the generation and development of the disease. As the primary regulator of the production and clearance of A $\beta$  and tau protein in AD, it has recently been discovered that the effect of autophagy on AD is related to its interaction with various signaling pathways and known AD biomarkers [2,8]. Therefore, exploring the autophagy-related biomarkers in AD from the perspective of pathway crosstalk has become the direction of our exploration.

First, we obtained the pathways with crosstalk in AD as well as the crosstalk genes on the pathways by the PAGA algorithm. We obtained 96 pathways with crosstalk, which further confirmed the extensive crosstalk between signaling pathways in AD. Then, by consulting the literature and annotating the autophagy genes of each pathway, 36 pathways were identified as autophagy-related crosstalk pathways. The genes on the pathways were identified as autophagy-related crosstalk genes and were reserved for further analysis. The results showed that autophagy-related crosstalk pathways in AD were mainly involved in the AD signaling pathway, mTOR signaling pathway, calcium signaling pathway, Wnt signaling pathway, apoptosis, insulin signaling pathway, neurotrophin signaling pathway, Type II diabetes mellitus, and other pathways.

These signaling pathways are closely related to the progression of AD. The mTOR signaling pathway is a crucial regulator of autophagy in AD. Previous studies have found that increasing mammalian target of mTOR signaling raises tau levels and phosphorylation [41]. Intracellular calcium signaling (Ca<sup>2+</sup>) pathway dysregulation is centrally involved in AD pathogenesis (the aggregation of pathogenic A $\beta$ , synapse loss and

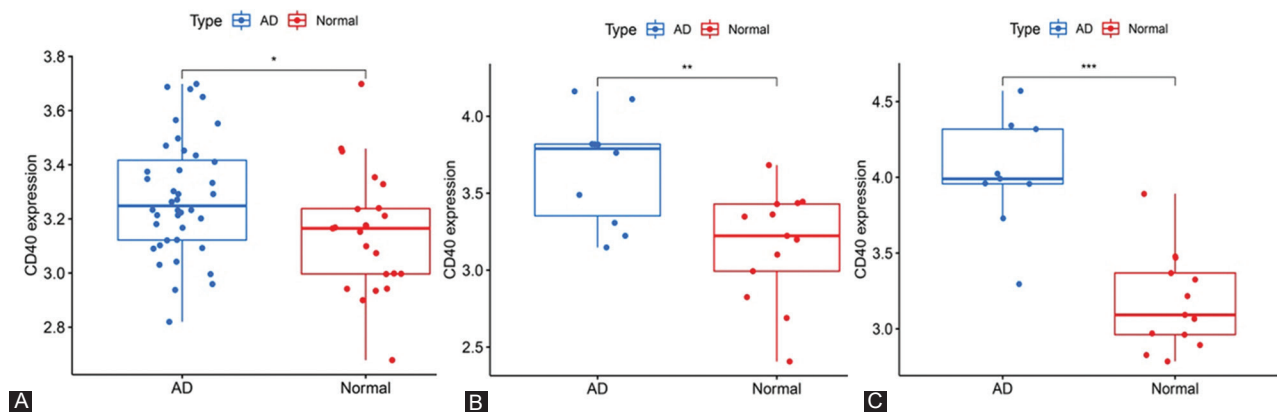


**FIGURE 8.** Relative expression levels of CD40 in Alzheimer's disease and control sample (“\*” represents  $p < 0.05$ , “\*\*” represents  $p < 0.01$ , “\*\*\*” represents  $p < 0.001$ ). (A) frontal cortex of GSE118553; (B) hippocampus of GSE5281; and (C) posterior cingulate of GSE5281.

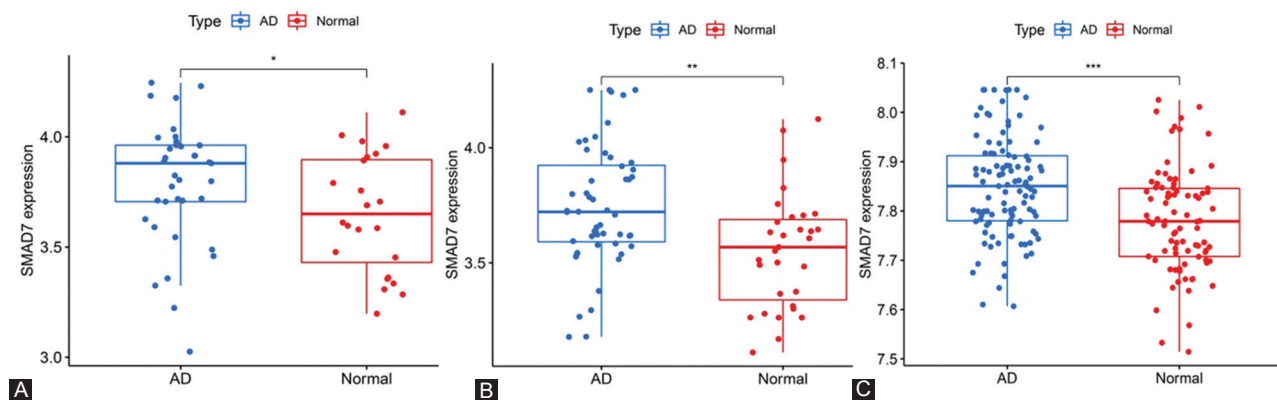


**FIGURE 9.** Relative expression levels of SMAD7 in Alzheimer's disease and control sample (“\*” represents  $p < 0.05$ , “\*\*” represents  $p < 0.01$ , “\*\*\*” represents  $p < 0.001$ ). (A) Entorhinal cortex of GSE118553; (B) temporal cortex of GSE118553; and (C) Syn4009614.

dysfunction and phosphorylation of tau) [34]. Furthermore, our results found that the calcium signaling pathway had a higher crosstalk score (pathway score = 0.57959). Multiple signaling pathways have been reported to play an important role in AD by regulating Ca<sup>2+</sup> homeostasis, including Wnt signaling pathway, neurotrophin signaling pathway and apoptosis [2].

The above results revealed that Ca<sup>2+</sup> might be involved in the occurrence and progression of AD through extensive crosstalk with other pathways. Insulin is a crucial factor regulating cell growth, autophagy, synaptic plasticity and cognitive function. Dysregulation of insulin signaling can cause neurofibrillary tangles and A $\beta$  plaques (the main pathological features of AD) [36]. The above results indicate that the pathways we screened and the crosstalk genes on the pathways play a crucial role in the AD occurrence, as well as pathological progression.

We also performed functional enrichment analysis of autophagy-related crosstalk genes obtained by WGCNA, which revealed that these autophagy-related crosstalk genes were mainly involved in PI3K-Akt signaling pathway, MAPK signaling pathway, calcium signaling pathway, insulin signaling pathway and neurotrophin signaling pathway. Previous studies have found that enhancing the PI3K-Akt signaling pathway in the central nervous system can improve memory function *in vivo* in mouse AD models and human trials [31]. MAPK signaling cascades play a role in mediating the AD-related pathological effects of apoE4 in the hippocampus [32]. The above results indicate that the crosstalk genes on the pathways also play a crucial role in ADs occurrence and pathological progression.

### Molecular biology analysis of autophagy-related prognostic genes

Multivariate Cox regression analysis was performed to construct a prognostic gene model based on two prognostic autophagy-related crosstalk genes (CD40 and SMAD7), which could predict the overall survival of AD patients with medium-to-high accuracy. The CD40 receptor is a member of the tumor necrosis factor superfamily of transmembrane receptors. A previous study found that the pathological features (such as amyloid burden, astrocytosis and microgliosis that are typical of AD-like pathology in these transgenic mouse strains) are reduced in mouse models deficient for CD40 compared with their littermates where CD40 is present [42]. In addition, the pattern of expression of CD40 has been reported to be altered in the brains of AD patients as well as in several animal models of AD [43].

In this study, the expression level of CD40 in AD patients was higher than that in controls, which indicated that high expression of CD40 was associated with AD pathological

progression. It has been suggested to play a role in A $\beta$  metabolism in AD [44]. Interaction of CD40 with its ligand CD40L mediates a broad range of immune and inflammatory responses in the periphery and in the central nervous system [45]. Innate immune and inflammatory responses play an important role in the accumulation and progression of amyloid in AD [46]. Dyad of CD40/CD40 ligand fosters neuroinflammation at the blood–brain barrier (BBB) and is regulated through JNK signaling [47]. The BBB plays a key role in the generation and maintenance of chronic inflammation during AD [48].

These combined evidence suggest that CD40 has a broad role in AD. Previous studies have reported that nuclear SMAD7 and TGF-beta1 levels were markedly upregulated in cortical brain regions of the TgCRND8 mice (a mouse model of familial AD) [49]. Moreover, TGF-beta1 may amplify A $\beta$  (1-42) (accumulation of the A $\beta$  peptide in the brain is a crucial factor in the development of AD)-mediated neurodegeneration in AD through SMAD7 and beta-catenin interaction and nuclear localization. Another study showed that inhibiting cellular SMAD7 levels significantly ameliorated the A $\beta$  (1-42)-mediated suppression of TGF-beta1-inducible transcription reporter activity, whereas SMAD7 transfection downregulated TGF-beta1-inducible transcription reporter activity [50]. Our results revealed that the expression level of SMAD7 was higher in AD patients than in controls, suggesting that inhibition of SMAD7 may be beneficial for AD.

Our study has some limitations. *In vivo* and *in vitro* experiments should be performed to further confirm our results. In summary, we performed comprehensive bioinformatics analysis and identified the autophagy-related prognostic gene signature containing two genes (CD40 and SMAD7) for AD patients.

### CONCLUSION

AD is a multifactor disease involving multiple signaling pathways, and the current methods for exploring new therapeutic targets need to be further enriched. Therefore, considering the core role of autophagy in AD and its interaction with other signaling pathways, this article provides a new method for mining autophagy-related biomarkers in AD. The molecular mechanism of autophagy in AD has not been explored from the perspective of pathway crosstalk. This article used the DESeq2 package to screen out differentially expressed lncRNAs.

The PAGA algorithm was used to explore the pathways related to AD, and the crosstalk pathways related to autophagy were screened through the number of autophagy genes in the pathways and literature. The mRNAs on the crosstalk pathways related to autophagy were reserved as feature mRNAs.

The WGCNA algorithm was used to extract the coexpression module of feature mRNAs and lncRNAs. Next, we applied clinical data to the genes in the coexpression module to obtain prognostic genes. Finally, CD40 and SMAD7 were identified as prognostic genes in AD. Based on the external AD dataset and literature, the role of the extracted prognostic genes in AD was confirmed. However, the exact mechanism underlying how these genes affected the prognosis of AD should be verified by more accurate experiments.

## ACKNOWLEDGMENTS

This work was supported by the Natural Science Foundation of Shanghai (No. 18ZR1417200) and the National Natural Science Foundation of China (No. 61803257).

We thank the patients' and their families' generous contributions to furthering understanding of AD. The results published here are in whole or in part based on data obtained from the AD Knowledge Portal (<https://adknowledgeportal.org>). Additional phenotypic data can be requested at [www.radc.rush.edu](http://www.radc.rush.edu).

## REFERENCES

- [1] Rabbito A, Dulewicz M, Kulczyńska-Przybik A, Mroczko B. Biochemical markers in Alzheimer's disease. *Int J Mol Sci* 2020;21(6):1989. <https://doi.org/10.3390/ijms21061989>
- [2] Gadhave K, Kumar D, Uversky VN, Giri R. A multitude of signaling pathways associated with Alzheimer's disease and their roles in AD pathogenesis and therapy. *Med Res Rev* 2020;41(5):2689-2745. <https://doi.org/10.1002/med.21719>
- [3] Uddin MS, Stachowiak A, Mamun AA, Tzvetkov NT, Takeda S, Atanasov AG, et al. Autophagy and Alzheimer's disease: From molecular mechanisms to therapeutic implications. *Front Aging Neurosci* 2018;10:4. <https://doi.org/10.3389/fnagi.2018.00004>
- [4] Caccamo A, Majumder S, Richardson A, Strong R, Oddo S. Molecular interplay between mammalian target of rapamycin (mTOR), amyloid-beta, and Tau: Effects on cognitive impairments. *J Biol Chem* 2010;285(17):13107-20. <https://doi.org/10.1074/jbc.M110.100420>
- [5] Nilsson P, Loganathan K, Sekiguchi M, Matsuba Y, Hui K, Tsubuki S, et al. A $\beta$  secretion and plaque formation depend on autophagy. *Cell Rep* 2013;5(1):61-9. <https://doi.org/10.1016/j.celrep.2013.08.042>
- [6] Salminen A, Kaamiranta K, Kauppinen A, Ojala J, Haapasalo A, Soininen H, et al. Impaired autophagy and APP processing in Alzheimer's disease: The potential role of Beclin 1 interactome. *Prog Neurobiol* 2013;106-107:33-54. <https://doi.org/10.1016/j.pneurobio.2013.06.002>
- [7] Wang X, Wang L. Screening and identification of potential peripheral blood biomarkers for Alzheimer's disease based on bioinformatics analysis. *Med Sci Monit* 2020;26:e924263. <https://doi.org/10.12659/MSM.924263>
- [8] Talebian S, Daghigh H, Yousefi B, Özkul Y, Ilkhani K, Seif F, et al. The role of epigenetics and non-coding RNAs in autophagy: A new perspective for thorough understanding. *Mech Ageing Dev* 2020;190:11309. <https://doi.org/10.1016/j.mad.2020.11309>
- [9] Kou X, Chen D, Chen N. The regulation of microRNAs in Alzheimer's disease. *Front Neurol* 2020;11:288. <https://doi.org/10.3389/fneur.2020.00288>
- [10] Moreno-García L, López-Royo T, Calvo AC, Toivonen JM, de la Torre M, Moreno-Martínez L, et al. Competing endogenous RNA networks as biomarkers in neurodegenerative diseases. *Int J Mol Sci* 2020;21(24):9582. <https://doi.org/10.3390/ijms21249582>
- [11] Xu X, Cui L, Zhong W, Cai Y. Autophagy-associated lncRNAs: Promising targets for neurological disease diagnosis and therapy. *Neural Plast* 2020;2020:8881687. <https://doi.org/10.1155/2020/8881687>
- [12] Wang J, Zhang Y, Marian C, Ransom HW. Identification of aberrant pathways and network activities from high-throughput data. *Brief Bioinform* 2012;13(4):406-19. <https://doi.org/10.1093/bib/bbs001>
- [13] Tian S, Wang C, Wang B. Incorporating pathway information into feature selection towards better performed gene signatures. *Biomed Res Int* 2019;2019:2497509. <https://doi.org/10.1155/2019/2497509>
- [14] Liu ZP, Wang Y, Zhang XS, Chen L. Identifying dysfunctional cross-talk of pathways in various regions of Alzheimer's disease brains. *BMC Syst Biol* 2010;4(Suppl 2):S11. <https://doi.org/10.1186/1752-0509-4-S2-S11>
- [15] Pálffy M, Reményi A, Korcsmáros T. Endosomal crosstalk: Meeting points for signaling pathways. *Trends Cell Biol* 2012;22(9):447-56. <https://doi.org/10.1016/j.tcb.2012.06.004>
- [16] Han J, Li C, Yang H, Xu Y, Zhang C, Ma J, et al. A novel dysregulated pathway-identification analysis based on global influence of within-pathway effects and crosstalk between pathways. *J R Soc Interface* 2015;12(102):20140937. <https://doi.org/10.1098/rsif.2014.0937>
- [17] Wang L, Li J, Zhao H, Hu J, Ping Y, Li F, et al. Identifying the cross-talk of dysfunctional pathways mediated by lncRNAs in breast cancer subtypes. *Mol Biosyst* 2016;12(3):711-20. <https://doi.org/10.1039/c5mb00700c>
- [18] Ma N, Tie C, Yu B, Zhang W, Wan J. Identifying lncRNA-miRNA-mRNA networks to investigate Alzheimer's disease pathogenesis and therapy strategy. *Aging (Albany NY)* 2020;12(3):2897-920. <https://doi.org/10.18632/aging.102785>
- [19] Niemira M, Collin F, Szalkowska A, Bielska A, Chwialkowska K, Reszec J, et al. Molecular signature of subtypes of non-small-cell lung cancer by large-scale transcriptional profiling: Identification of key modules and genes by weighted gene co-expression network analysis (WGCNA). *Cancers (Basel)* 2019;12(1):37. <https://doi.org/10.3390/cancers12010037>
- [20] Mostafavi S, Gaiteri C, Sullivan SE, White CC, Tasaki S, Xu J, et al. A molecular network of the aging human brain provides insights into the pathology and cognitive decline of Alzheimer's disease. *Nat Neurosci* 2018;21(6):811-9. <https://doi.org/10.1038/s41593-018-0154-9>
- [21] Bennett DA, Buchman AS, Boyle PA, Barnes LL, Wilson RS, Schneider JA. Religious orders study and rush memory and aging project. *J Alzheimers Dis* 2018;64(S1):S161-S189. <https://doi.org/10.3233/JAD-179939>
- [22] Love MI, Huber W, Anders S. Moderated estimation of fold change and dispersion for RNA-seq data with DESeq2. *Genome Biol* 2014;15(12):550. <https://doi.org/10.1186/s13059-014-0550-8>
- [23] Li C, Han J, Yao Q, Zou C, Xu Y, Zhang C, Shang D, et al. Identification of metabolic subpathways via joint power of interesting genes and metabolites and their topologies within pathways. *Nucleic Acids Res* 2013;41(9):e101. <https://doi.org/10.1093/nar/gkt161>
- [24] Li C, Li X, Miao Y, Wang Q, Jiang W, Xu C, et al. SubpathwayMiner: A software package for flexible identification of pathways. *Nucleic Acids Res* 2009;37(19):e131. <https://doi.org/10.1093/nar/gkp667>
- [25] Zhang J, Suo Y, Liu M, Xu X. Identification of genes related to proliferative diabetic retinopathy through RWR algorithm based on protein-protein interaction network. *Biochim Biophys Acta Mol Basis*

- Dis 2018;1864(6 Pt B):2369-75.  
<https://doi.org/10.1016/j.bbadis.2017.11.017>
- [26] Li Z, Xiao Y, Xu L, Wang Q. Mining the key genes for ventilator-induced lung injury using co-expression network analysis. *Biosci Rep* 2021;41(3):BSR20203235.  
<https://doi.org/10.1042/BSR20203235>
- [27] Yu P, Lan H, Song X, Pan Z. High expression of the SH3TC2-DT/SH3TC2 gene pair associated with FLT3 mutation and poor survival in acute myeloid leukemia: An integrated TCGA analysis. *Front Oncol* 2020;10:829.  
<https://doi.org/10.3389/fonc.2020.00829>
- [28] Tian Z, He W, Tang J, Liao X, Yang Q, Wu Y, et al. Identification of important modules and biomarkers in breast cancer based on WGCNA. *Onco Targets Ther* 2020;13:6805-17.  
<https://doi.org/10.2147/OTT.S258439>
- [29] Kanehisa M, Furumichi M, Tanabe M, Sato Y, Morishima K. KEGG: New perspectives on genomes, pathways, diseases and drugs. *Nucleic Acids Res* 2017;45(D1):D353-61.  
<https://doi.org/10.1093/nar/gkw1092>
- [30] Huang DW, Sherman BT, Tan Q, Collins JR, Alvord WG, Roayaei J, et al. The DAVID gene functional classification tool: A novel biological module-centric algorithm to functionally analyze large gene lists. *Genome Biol* 2007;8(9):R183.  
<https://doi.org/10.1186/gb-2007-8-9-r183>
- [31] Gabbouj S, Ryhänen S, Marttinen M, Wittrahm R, Takalo M, Kempainen S, et al. Altered insulin signaling in Alzheimer's disease brain special emphasis on PI3K-Akt pathway. *Front Neurosci* 2019;13:629.  
<https://doi.org/10.3389/fnins.2019.00629>
- [32] Salomon-Zimri S, Koren A, Angel A, Ben-Zur T, Offen D, Michaelson DM. The role of MAPK's signaling in mediating ApoE4-driven pathology *in vivo*. *Curr Alzheimer Res* 2019;16(4):281-92.  
<https://doi.org/10.2174/1567205016666190228120254>
- [33] Plácido AI, Pereira CM, Duarte AI, Candeias E, Correia SC, Santos RX, et al. The role of endoplasmic reticulum in amyloid precursor protein processing and trafficking: Implications for Alzheimer's disease. *Biochim Biophys Acta* 2014;1842(9):1444-53.  
<https://doi.org/10.1016/j.bbadis.2014.05.003>
- [34] Mustaly-Kalimi S, Littlefield AM, Stutzmann GE. Calcium signaling deficits in glia and autophagic pathways contributing to neurodegenerative disease. *Antioxid Redox Signal* 2018;29(12):1158-1175.  
<https://doi.org/10.1089/ars.2017.7266>
- [35] Lee S, Salazar SV, Cox TO, Strittmatter SM. Pyk2 Signaling through grafi and RhoA GTPase is required for amyloid- $\beta$  oligomer-triggered synapse loss. *J Neurosci* 2019;39(10):1910-29.  
<https://doi.org/10.1523/JNEUROSCI.2983-18.2018>
- [36] Akhtar A, Sah SP. Insulin signaling pathway and related molecules: Role in neurodegeneration and Alzheimer's disease. *Neurochem Int* 2020;135:104707.  
<https://doi.org/10.1016/j.neuint.2020.104707>
- [37] Mitre M, Mariga A, Chao MV. Neurotrophin signalling: Novel insights into mechanisms and pathophysiology. *Clin Sci (Lond)* 2017;131(1):13-23.  
<https://doi.org/10.1042/CS20160044>
- [38] Pelucchi S, Stringhi R, Marcello E. Dendritic spines in Alzheimer's disease: How the actin cytoskeleton contributes to synaptic failure. *Int J Mol Sci* 2020;21(3):908.  
<https://doi.org/10.3390/ijms21030908>
- [39] Colacurcio DJ, Pensalfini A, Jiang Y, Nixon RA. Dysfunction of autophagy and endosomal-lysosomal pathways: Roles in pathogenesis of Down syndrome and Alzheimer's disease. *Free Radic Biol Med* 2018;114:40-51.  
<https://doi.org/10.1016/j.freeradbiomed.2017.10.001>
- [40] Kirouac L, Rajic AJ, Cribbs DH, Padmanabhan J. Activation of ras-ERK signaling and GSK-3 by amyloid precursor protein and amyloid beta facilitates neurodegeneration in Alzheimer's disease. *eNeuro* 2017;4(2):ENEURO.0149-16.2017.  
<https://doi.org/10.1523/ENEURO.0149-16.2017>
- [41] Uddin MS, Mamun AA, Labu ZK, Hidalgo-Lanussa O, Barreto GE, Ashraf GM. Autophagic dysfunction in Alzheimer's disease: Cellular and molecular mechanistic approaches to halt Alzheimer's pathogenesis. *J Cell Physiol* 2019;234(6):8094-112.  
<https://doi.org/10.1002/jcp.27588>
- [42] Laporte V, Ait-Ghezala G, Volmar CH, Mullan M. CD40 deficiency mitigates Alzheimer's disease pathology in transgenic mouse models. *J Neuroinflamm* 2006;3:3.  
<https://doi.org/10.1186/1742-2094-3-3>
- [43] Tan J, Town T, Suo Z, Wu Y, Song S, Kundtz A, et al. Induction of CD40 on human endothelial cells by Alzheimer's beta-amyloid peptides. *Brain Res Bull* 1999;50(2):143-8.  
[https://doi.org/10.1016/s0361-9230\(99\)00122-7](https://doi.org/10.1016/s0361-9230(99)00122-7)
- [44] Buchhave P, Janciauskiene S, Zetterberg H, Blennow K, Minthon L, Hansson O. Elevated plasma levels of soluble CD40 in incipient Alzheimer's disease. *Neurosci Lett* 2009;450(1):56-9.  
<https://doi.org/10.1016/j.neulet.2008.10.091>
- [45] Ait-Ghezala G, Volmar CH, Frieling J, Paris D, Tweed M, Bakshi P, et al. CD40 promotion of amyloid beta production occurs via the NF-kappaB pathway. *Eur J Neurosci* 2007;25(6):1685-95.  
<https://doi.org/10.1111/j.1460-9568.2007.05424.x>
- [46] Ho GJ, Dreger R, Hakimian E, Maslah E. Mechanisms of cell signaling and inflammation in Alzheimer's disease. *Curr Drug Targets Inflamm Allergy* 2005;4(2):247-56.  
<https://doi.org/10.2174/1568010053586237>
- [47] Ramirez SH, Fan S, Dykstra H, Reichenbach N, Del Valle L, Potula R, et al. Dyad of CD40/CD40 ligand fosters neuroinflammation at the blood-brain barrier and is regulated via JNK signaling: implications for HIV-1 encephalitis. *J Neurosci* 2010;30(28):9454-64.  
<https://doi.org/10.1523/JNEUROSCI.5796-09.2010>
- [48] Zenaro E, Piacentino G, Constantin G. The blood-brain barrier in Alzheimer's disease. *Neurobiol Dis* 2017;107:41-56.  
<https://doi.org/10.1016/j.nbd.2016.07.007>
- [49] Salins P, He Y, Olson K, Glazner G, Kashour T, Amara F. TGF-beta1 is increased in a transgenic mouse model of familial Alzheimer's disease and causes neuronal apoptosis. *Neurosci Lett* 2008;430(1):81-6.  
<https://doi.org/10.1016/j.neulet.2007.10.025>
- [50] Lee EO, Kang JL, Chong YH. The amyloid-beta peptide suppresses transforming growth factor-beta1-induced matrix metalloproteinase-2 production via Smad7 expression in human monocytic THP-1 cells. *J Biol Chem* 2005;280(9):7845-53.  
<https://doi.org/10.1074/jbc.M409101200>

## Related articles published in BJBMS

- miR-212-3p attenuates neuroinflammation of rats with Alzheimer's disease via regulating the SP1/BACE1/NLRP3/Caspase-1 signaling pathway  
Wei Nong et al., BJBMS, 2022
- Asymptomatic neurotoxicity of amyloid  $\beta$ -peptides (A $\beta$ 1-42 and A $\beta$ 25-35) on mouse embryonic stem cell-derived neural cells  
Nur Izzati Mansor et al., BJBMS, 2021
- Neural stem cell-conditioned medium ameliorates A $\beta$ 25-35-induced damage in SH-SY5Y cells by protecting mitochondrial function  
Guoyong Jia et al., BJBMS, 2021

## SUPPLEMENTAL DATA

SUPPLEMENTAL TABLE 1. Top 30 differential genes

Id	log2FC	p-value	padj	Regulate
<i>AC009063.2</i>	0.770513051	1.63E-10	4.09E-07	Upregulated
<i>AC008737.3</i>	0.932512925	4.95E-10	7.46E-07	Upregulated
<i>AL450313.1</i>	1.79036646	1.16E-09	1.45E-06	Upregulated
<i>LINC01736</i>	0.810530425	1.09E-08	1.02E-05	Upregulated
<i>AC243964.2</i>	1.221925555	1.62E-08	1.36E-05	Upregulated
<i>LINC02172</i>	0.751632155	1.32E-07	5.25E-05	Upregulated
<i>AL390066.1</i>	0.561995855	4.48E-07	0.000116451	Upregulated
<i>LINC01134</i>	0.667604638	6.04E-07	0.000142305	Upregulated
<i>LINC01445</i>	0.569507479	8.44E-07	0.00019293	Upregulated
<i>AC002428.2</i>	0.819012877	1.25E-06	0.000244382	Upregulated
<i>AP003117.1</i>	0.539248872	1.26E-06	0.000244382	Upregulated
<i>AC127496.1</i>	0.588155825	4.09E-06	0.000512292	Upregulated
<i>AL355974.3</i>	0.660144797	1.29E-05	0.001148947	Upregulated
<i>LINC02397</i>	0.968817228	2.11E-05	0.001638011	Upregulated
<i>AC092155.1</i>	0.777738272	2.27E-05	0.001708868	Upregulated
<i>ERVH-1</i>	-0.762166936	2.89E-10	5.45E-07	Downregulated
<i>FAM225B</i>	-1.055485404	2.06E-08	1.42E-05	Downregulated
<i>AC015819.3</i>	-0.704015057	3.61E-08	2.01E-05	Downregulated
<i>AC016576.1</i>	-1.003937063	1.53E-07	5.50E-05	Downregulated
<i>AC010266.2</i>	-0.551501253	1.93E-07	6.13E-05	Downregulated
<i>AC016205.1</i>	-0.736957053	3.63E-07	0.000104717	Downregulated
<i>AC018541.1</i>	-1.022992779	1.11E-06	0.000238355	Downregulated
<i>LINC01844</i>	-0.555035901	1.45E-06	0.000270919	Downregulated
<i>AC074351.1</i>	-0.822739102	2.19E-06	0.000366291	Downregulated
<i>LINC01476</i>	-0.567521021	3.53E-06	0.000480776	Downregulated
<i>AL353608.3</i>	-0.620152796	3.57E-06	0.000480776	Downregulated
<i>LINC00507</i>	-0.551519082	3.92E-06	0.000501233	Downregulated
<i>LINC01007</i>	-0.62218615	4.14E-06	0.000512292	Downregulated
<i>LINC02296</i>	-0.686097709	4.89E-06	0.000562348	Downregulated
<i>AC010425.1</i>	-0.793469236	7.74E-06	0.000748242	Downregulated

SUPPLEMENTAL TABLE 2. Thirty-six autophagy-related pathways

Pathway name	Size	Pathway ID	Pathway score	Autophagy
Pathways in cancer	268	path: hsa05200	0.43999	39
Protein processing in endoplasmic reticulum	152	path: hsa04141	0.44823	27
MAPK signaling pathway	219	path: hsa04010	0.51284	20
Apoptosis	70	path: hsa04210	0.44783	17
ErbB signaling pathway	78	path: hsa04012	0.53336	16
Focal adhesion	167	path: hsa04510	0.54818	16
Hepatitis C	99	path: hsa05160	0.46977	16
Insulin signaling pathway	119	path: hsa04910	0.51274	16
mTOR signaling pathway	46	path: hsa0415	0.48142	16
Neurotrophin signaling pathway	114	path: hsa04722	0.54769	15
Chronic myeloid leukemia	68	path: hsa05220	0.46647	14
Toll-like receptor signaling pathway	63	path: hsa04620	0.42614	14
Alzheimer's disease	132	path: hsa05010	0.42487	13
Chagas disease	80	path: hsa05142	0.50219	13
Chemokine signaling pathway	118	path: hsa04062	0.54436	12
Colorectal cancer	60	path: hsa05210	0.56606	12
NOD-like receptor signaling pathway	45	path: hsa04621	0.53817	12
Small cell lung cancer	76	path: hsa05222	0.41707	12
RIG-I-like receptor signaling pathway	47	path: hsa04622	0.50676	11
Endocytosis	174	path: hsa04144	0.42422	10
Glioma	58	path: hsa05214	0.57765	10
Phagosome	110	path: hsa04145	0.49985	10
Regulation of actin cytoskeleton	165	path: hsa04810	0.54832	10
Adipocytokine signaling pathway	54	path: hsa04920	0.57427	9

(Contd...)

**SUPPLEMENTAL TABLE 2.** (Continued)

Pathway name	Size	Pathway ID	Pathway score	Autophagy
Endometrial cancer	48	path: hsa05213	0.53481	9
GnRH signaling pathway	78	path: hsa04912	0.56101	9
B-cell receptor signaling pathway	58	path: hsa04662	0.58792	8
T-cell receptor signaling pathway	76	path: hsa04660	0.55474	8
Long-term depression	54	path: hsa04730	0.60749	6
Type II diabetes mellitus	32	path: hsa04930	0.5506	6
Long-term potentiation	64	path: hsa04720	0.68263	5
Wnt signaling pathway	123	path: hsa04310	0.4932	5
Calcium signaling pathway	133	path: hsa04020	0.57959	4
Pancreatic cancer	62	path: hsa05212	0.56527	16
Toxoplasmosis	102	path: hsa05145	0.46928	15
Prostate cancer	76	path: hsa05215	0.50957	18

**SUPPLEMENTAL TABLE 3.** Crosstalk genes and their crosstalk scores on 10 autophagy-related crosstalk pathways

Alzheimer's disease	Calcium signaling pathway	Insulin signaling pathway	Neurotrophin signaling pathway				
<i>PLCB3</i>	0.537	ITPKB	0.547	PRKX	0.709	NFKBIA	0.452
<i>CALM3</i>	0.488	PRKX	0.709	TRIP10	0.499	PIK3R5	0.619
<i>PLCB1</i>	0.491	PRKCG	0.581	RHOQ	0.467	CAMK4	0.357
<i>CALM2</i>	0.468	MYLK3	0.444	PIK3R5	0.619	MAPK8	0.56
<i>ITPR1</i>	0.406	PLCB3	0.537	PRKACA	0.62	MAPKAPK2	0.362
<i>CACNA1D</i>	0.396	TRPC1	0.42	MAPK8	0.56	CALM3	0.488
<i>PPP3R1</i>	0.395	CCKBR	0.38	PRKAG1	0.391	YWHAZ	0.346
<i>CALM1</i>	0.455	TACR2	0.373	PTPRF	0.358	SHC1	0.378
<i>MAPK1</i>	0.729	PRKACA	0.62	CALM3	0.488	MAPK14	0.648
<i>CASP9</i>	0.366	P2RX7	0.402	PRKCI	0.459	CDC42	0.547
<i>PSEN2</i>	0.334	CAMK4	0.357	SHC1	0.378	CALM2	0.468
<i>NOS1</i>	0.314	PDGFRB	0.437	CALM2	0.468	RP56KA1	0.34
<i>GRIN2A</i>	0.343	CALM3	0.488	INPP5D	0.349	KRAS	0.516
<i>SDHB</i>	0.323	PLCB1	0.491	PRKAB1	0.36	NRAS	0.504
<i>NDUFA5</i>	0	CALM2	0.468	KRAS	0.516	CALM1	0.455
<i>PPP3CB</i>	0.37	HTR5A	0.316	NRAS	0.504	MAPK12	0.635
<i>GRIN2D</i>	0.337	ERBB3	0.411	PRKACB	0.577	YWHAZ	0.309
<i>ATP2A2</i>	0.329	TBXA2R	0.317	CALM1	0.455	MAPK1	0.729
<i>GSK3B</i>	0.404	ITPR1	0.406	PCK1	0.396	MAPK10	0.517
<i>GAPDH</i>	0.35	CACNA1D	0.396	MAPK1	0.729	PSEN2	0.334
<i>SDHC</i>	0.308	PRKACB	0.577	MAPK10	0.517	AKT3	0.453
<i>NAE1</i>	0.294	PPP3R1	0.395	PRKAA2	0.353	BRAF	0.355
<i>MAPT</i>	0.304	CALM1	0.455	AKT3	0.453	CAMK2D	0.336
<i>UQCRI10</i>	0	ADRA1D	0.315	BRAF	0.355	YWHAQ	0.288
<i>CDK5R1</i>	0.343	ADCY1	0.407	HK1	0.476	GSK3B	0.404
<i>APP</i>	0.392	VDAC1	0.35	GSK3B	0.404	MAPK9	0.499
<i>UQCRC2</i>	0	NOS1	0.314	MAPK9	0.499	BDNF	0.271
<i>NDUFB5</i>	0	GRIN2A	0.343	PYGB	0.328	MAGED1	0.262
<i>APH 1A</i>	0.258	SLC8A2	0.337	PYGM	0.328	YWHAZ	0.27
<i>GRIN2B</i>	0.312	CAMK2D	0.336	PRKAR1A	0.276	TRAF6	0.415
<i>NDUFA6</i>	0	PTAFR	0.288	RHEB	0.337	SHC3	0.315
<i>SDHD</i>	0.278	CACNA1E	0.365	FLOT2	0.264	RP56KA6	0.282
<i>NDUFA10</i>	0	PPP3CB	0.37	SHC3	0.315	MAP2K5	0.267
<i>COX8A</i>	0	GRIN2D	0.337	PTPN1	0.246	IRAK2	0.267
<i>NDUFC2</i>	0	ATP2A2	0.329	MAP2K1	0.314	KIDINS220	0.252
<i>SDHA</i>	0.273	ATP2B2	0.323	EIF4E2	0.261	ARHGDI1A	0.255
<i>PPP3CA</i>	0.322	CHRM1	0.281	PIK3R1	0.511	CAMK2A	0.295
<i>NDUFA9</i>	0	ERBB4	0.521	PRKAR1B	0.237	MAP2K1	0.314
<i>CYCS</i>	0.319	VDAC2	0.323	GRB2	0.321	NGFR	0.446
<i>ADAM17</i>	0.247	ATP2B3	0.317	TSC1	0.245	YWHAZ	0.242
<i>COX7B</i>	0	PTK2B	0.346	PDPK1	0.303	NFKBIB	0.26
<i>COX7A2L</i>	0	HRH2	0.257	PRKCH	0.365	PIK3R1	0.511
<i>NDUFC1</i>	0	ATP2B1	0.303	IKKB	0.34	GRB2	0.321
<i>CAPN2</i>	0.242	GRM5	0.327	EIF4EBP1	0.259	NTRK3	0.255

(Contd...)

**SUPPLEMENTAL TABLE 3. (Continued)**

Alzheimer's disease		Calcium signaling pathway		Insulin signaling pathway		Neurotrophin signaling pathway	
<i>COX6B1</i>	0	CACNA1B	0.336	ACACB	0.295	IKBKB	0.34
<i>CASP7</i>	0.245	CACNA1G	0.334	PRKAR2B	0.216	MAP2K7	0.453
<i>NDUFV1</i>	0	NOS2	0.316	PHKB	0.229	HRAS	0.42
<i>SNCA</i>	0	SLC8A3	0.296	SOCS4	0.28	RAC1	0.616
<i>CACNA1F</i>	0.276	CAMK2A	0.295	HRAS	0.42	GAB1	0.221
<i>GNAQ</i>	0.45	CHRM3	0.247	SH2B2	0.213	MAPK13	0.565
<i>ATP2A3</i>	0.251	HTR2A	0.238	MKNK1	0.246	SH2B2	0.213
<i>APBB1</i>	0.228	GNAS	0.529	HK2	0.406	YWHAB	0.209
<i>NCSTN</i>	0.212	CHRM2	0.238	INSR	0.245	PIK3CB	0.468
<i>NDUFAB1</i>	0	PPP3CA	0.322	PPARGC1A	0.2	RIPK2	0.391
<i>NDUFB6</i>	0	PDE1B	0.269	PIK3CB	0.468	PDK1	0.196
<i>COX7A2</i>	0	ADCY2	0.325	PRKAG2	0.24	RELA	0.395
<i>NDUFA4</i>	0	CD38	0.275	PHKG2	0.208	SH2B1	0.194
<i>ATF6</i>	0.216	P2RX6	0.265	PPP1CA	0.258	MAPK3	0.658
<i>NDUFS1</i>	0	VDAC3	0.274	MAPK3	0.658	CSK	0.276
<i>NDUFS6</i>	0	PDE1A	0.26	MTOR	0.367	RPS6KA5	0.19
<i>NDUFS4</i>	0	ADRA1B	0.223	PPP1R3B	0.198	MAPK11	0.549
<i>NDUFB4</i>	0	PHKB	0.229	PPP1R3C	0.197	BCL2	0.233
<i>UQCRCQ</i>	0	SLC25A5	0.261	EXOC7	0.196	SOS1	0.291
<i>UQCRCR</i>	0	CACNA1F	0.276	LIPE	0.228	RPS6KA3	0.191
<i>NDUFA2</i>	0	TACR1	0.207	PPP1CC	0.244	PLCG1	0.341
<i>MAPK3</i>	0.658	PRKCB	0.372	EIF4E	0.197	NFKB1	0.372
<i>BACE1</i>	0	GNAQ	0.45	SOS1	0.291	RHOA	0.438
<i>CYC1</i>	0	SPHK1	0.236	PRKAB2	0.212	RAP1A	0.252
<i>UQCRCF1</i>	0	PPID	0.26	ACACA	0.251	CRK	0.306
<i>COX6C</i>	0	ATP2A3	0.251	RPS6KB1	0.214	NTRK2	0.199
<i>PPP3CC</i>	0.279	GRM1	0.269	RPTOR	0	FOXO3	0.121
<i>CDK5</i>	0.23	SLC25A4	0.25	TSC2	0.315	NFKBIE	0.133
<i>COX5A</i>	0	SLC8A1	0.241	FOXO1	0.19	ZNF274	0.115
<i>NDUFS3</i>	0	PHKG2	0.208	PPP1CB	0.224	RAP1B	0.224
<i>NDUFA3</i>	0	GNAL	0.342	PDE3B	0.255	PIK3CD	0.404
<i>COX7C</i>	0	RYR2	0.249	PCK2	0.254	ABL1	0.24
<i>CACNA1C</i>	0.278	ADCY7	0.287	ELK1	0.224	IRAK1	0.172
<i>COX4I1</i>	0	PPP3CC	0.279	CRK	0.306	MAP2K2	0.193
<i>LPL</i>	0.223	PLCE1	0.269	SREBF1	0.165	SOS2	0.228
<i>PLCB4</i>	0.361	CACNA1C	0.278	CBLB	0.238	IRAK4	0.159
<i>NDUFB11</i>	0	PLCB4	0.361	FASN	0.173	PRDM4	0.0928
<i>NDUFB3</i>	0	PDE1C	0.212	RPS6KB2	0.173	AKT1	0.288
<i>NDUFA12</i>	0	PLCG1	0.341	PDE3A	0.226	JUN	0.158
<i>COX5B</i>	0	P2RX5	0.201	PHKG1	0.134	RPS6KA4	0.0942
<i>NDUFA1</i>	0	ATP2B4	0.201	PIK3CD	0.404	FRS2	0.0778
<i>NDUFS5</i>	0	GNA14	0.375	SORBS1	0.209	IRAK3	0.0954
<i>UQCRC1</i>	0	NTSR1	0.151	MAP2K2	0.193	RPS6KA2	0.101
<i>NDUFA8</i>	0	TNNC2	0.204	GYS1	0.148	MAPK7	0.143
<i>NDUFB2</i>	0	CACNA1H	0.219	PRKAA1	0.174	SORT1	0.0689
<i>GRIN1</i>	0.257	PRKCA	0.323	PYGL	0.17	CALML6	0.256
<i>IDE</i>	0	ADCY4	0.262	SOS2	0.228	BAX	0.0914
<i>CAPN1</i>	0.165	GRIN1	0.257	AKT1	0.288	PTPN11	0.0838
<i>NDUFV3</i>	0	PLCD3	0.284	HK3	0.315	MAP3K1	0.333
<i>UQCRB</i>	0	ADCY3	0.277	PRKAR2A	0.08	RAPGEF1	0.0913
<i>NDUFS7</i>	0	CACNA1A	0.229	RPS6	0.0767	MAP3K5	0.163
<i>APAF1</i>	0.133	ERBB2	0.168	CALML6	0.256	AKT2	0.25
<i>NDUFB10</i>	0	PHKG1	0.134	SOCS3	0.145	CRKL	0.228
<i>NDUFS2</i>	0	ADRB1	0.134	PHKA2	0.0812	SHC4	0.116
<i>NDUFB7</i>	0	OXTR	0.108	FLOT1	0.0593	ARHGDIIB	0.0556
<i>NDUFB8</i>	0	CYSLTR2	0.0993	RAPGEF1	0.0913	PIK3CA	0.353
<i>CASP3</i>	0.236	GNA15	0.328	CBL	0.168	IRS1	0.114
<i>FAS</i>	0.125	EDNRA	0.0949	AKT2	0.25	BAD	0.127
<i>NDUFS8</i>	0	ITPKA	0.17	CRKL	0.228	SH2B3	0.0405

(Contd...)

**SUPPLEMENTAL TABLE 3. (Continued)**

Alzheimer's disease		Calcium signaling pathway		Insulin signaling pathway		Neurotrophin signaling pathway	
NDUFB1	0	ADCY8	0.223	GCK	0.123	PSEN1	0.0927
NDUFA4L2	0	P2RX4	0.128	SHC4	0.116	CAMK2G	0.0927
UQCRHL	0	PDGFRA	0.249	PIK3CA	0.353	RAF1	0.103
LRP1	0.107	ADORA2B	0.0724	IRS1	0.114	CAMK2B	0.0775
UQCR11	0	EGFR	0.296	SLC2A4	0.198	PLCG2	0.21
ERN1	0.141	RYR3	0.137	BAD	0.127	MAP3K3	0.0554
CASP8	0.157	MYLK	0.134	SOCS2	0.116	ATF4	0.166
BACE2	0	CALML6	0.256	PHKA1	0.0525	SHC2	0.0791
TNFRSF1A	0.125	HRH1	0.0627	MKNK2	0.0757	TP53	0.895
PSENE1	0.0977	PHKA2	0.0812	RAF1	0.103	IRS2	0.079
RYR3	0.137	NOS3	0.0798	PPP1R3D	0.0376	PIK3R3	0.329
BID	0.0755	PLCD1	0.204	SHC2	0.0791		
CALML6	0.256	ITPR3	0.143	EIF4E1B	0.0421		
HSD17B10	0.0902	EDNRB	0.0479	IRS2	0.079		
NDUFA13	0	CAMK2G	0.0927	PIK3R3	0.329		
ITPR3	0.143	PHKA1	0.0525	ARAF	0.0631		
FADD	0.155	CACNA11	0.105				
APOE	0.0494	PLCB2	0.237				
BAD	0.127	DRD1	0.0298				
ADAM10	0.0387	ADRA1A	0.0346				
NDUFA11	0	GRIN2C	0.0868				
COX6A1	0	SPHK2	0.0557				
PSEN1	0.0927	ADCY9	0.136				
PLCB2	0.237	PLCD4	0.176				
COX7A1	0	CAMK2B	0.0775				
GRIN2C	0.0868	ITPR2	0.114				
ITPR2	0.114	RYR1	0.0793				
ATP2A1	0.0671	PLCG2	0.21				
		ATP2A1	0.0671				
		GNA11	0.258				

**SUPPLEMENTAL TABLE 4. Genes associated with other diseases**

Disease	Gene
Mitochondrial complex I deficiency	<i>NDUFA11; NDUFS7; NDUFS4; NDUFS8; NDUFV1; NDUFS1; NDUFS2; NDUFS3; NDUFS6; NDUFA1; NDUFA2; NDUFA10; NDUFB9; NDUFB3; NDUFA9; NDUFB8; NDUFA6; NDUFB10; NDUFC2; NDUFA8; NDUFA13; NDUFA12; NDUFB11</i>
Colorectal cancer	<i>CTNNB1; DCC; APC; MSH6; KRAS; SMAD4; MLH1; MSH2; MSH3; SMAD2; PIK3CA; BAX; CCND1; TGFA; TGFB2; BRAF; TP53; AXIN2</i>
Hepatocellular carcinoma	<i>CDKN2A; CTNNB1; HGF; IGF1R; MET; MYC; NFE2L2; PIK3CA; RBL1; PTEN; TGFA; TGFB2; TP53; FZD7; AXIN1; CASP8</i>
Autosomal dominant intellectual developmental disorder	<i>CACNG2; CTNNB1; CLTC; AP2M1; DYNC1H1; GRIN2B; GRIN1; GNB1; MEF2C; PPP2R5D; PPP2R1A; RAC1; TBL1XR1; CAMK2A; CAMK2B; CAMK2G</i>
Gastric cancer	<i>CDKN1B; CTNNB1; ERBB2; FGFR2; APC; KRAS; MET; MLH1; NRAS; PIK3CA; RARB; TGFB1; TP53; CCNE1; CDH1</i>
Thyroid cancer	<i>TFG; TPM3; CTNNB1; HRAS; KRAS; NRAS; PPARG; RET; CCDC6; NCOA4; BRAF; TPR; TP53; CDH1</i>
Diffuse large B-cell lymphoma	<i>GNA13; CDKN2A; CDKN2B; CREBBP; EP300; GNA12; FOXO1; MYC; MYD88; PTEN; BCL2; TNFAIP3; TP53; CARD11</i>
Early infantile epileptic encephalopathy	<i>DNM1; FGF12; FGF13; PLCB1; CYFIP2; GNAO1; GRIN2B; GRIN2D; NTRK2; ATP6V1A; PPP3CA; CACNA1A; YWHAG; CACNA1E</i>
Non-small-cell lung cancer	<i>CDKN2A; RASSF1; EGFR; FHIT; KRAS; IRF1; MET; PIK3CA; PPP2R1B; RET; BRAF; TP53</i>
Dilated cardiomyopathy	<i>CRYAB; HLA-DRB1; HLA-DPA1; HLA-DPB1; HLA-DQA1; HLA-DQB1; LAMA4; PSEN1; PSEN2; RAF1; SDHA; VCL; ACTN2</i>
Noonan syndrome and related disorders	<i>HRAS; KRAS; ARAF; NF1; NRAS; MAP2K1; MAP2K2; PPP1CB; PTPN11; SOS1; BRAF; SOS2; CBL</i>
Glioma	<i>CDK4; CDKN2A; ERBB2; EGFR; MDM2; PDGFA; PDGFB; PDGFRA; PDGFRB; PTEN; RBL1; TP53</i>
Medulloblastoma	<i>APC; APC2; CTNNB1; MYC; MDM2; SUFU; PTCH1; SMO; TP53; PTCH2; AXIN1; AXIN2</i>
Esophageal cancer	<i>CDKN2A; EGFR; DCC; APC; EAS; NOS2; PTGS2; RBL1; TGFB2; TP53</i>
Ovarian cancer	<i>CTNNB1; ERBB2; AKT2; AKT1; KRAS; MSH2; MLH1; MYC; PIK3CA; TP53; CDH1</i>
Chronic myeloid leukemia	<i>CDKN2A; MECOM; BCR; ABL1; RBL1; TP53; RUNX1</i>
Alzheimer's disease	<i>ADAM10; APP; APOE; PSEN1; PSEN2</i>
Endometrial cancer	<i>CTNNB1; ERBB2; KRAS; MLH1; MSH3; PTEN; TP53; CDH1</i>
Pancreatic cancer	<i>CDKN2A; ERBB2; KRAS; SMAD4; STK11; TP53</i>
Prostate cancer	<i>CDKN1B; ELK4; AR; NKX3-1; PTEN</i>
Type II diabetes mellitus	<i>CDKN2A; CDKN2B; KCNJ11; PPARG; TCF7L2; WFS1</i>
Small-cell lung cancer	<i>FHIT; MYC; PPP2R1B; BCL2; RBL1; PTEN; TP53</i>

**SUPPLEMENTAL TABLE 5.** Definition of survival time and survival status of AD patients. Because the age of patients over 90 years old in the clinical data is shown as 90+, we set the observation starting point as the time of diagnosis of each patient and the observation ending point as 90 years old. The survival status of patients with a death age of 90 + is alive, while the survival status of patients with a death age of less than 90 is dead, and the survival time of 82 patients was finally obtained. The clinical data downloaded from the AMP-AD database were sorted and screened, and then, the survival time and clinical characteristics (braaksc, ceradsc, and dcfdx\_iv: Clinical cognitive diagnosis summary at last visit) of 82 patients were obtained

Endocytosis		Protein processing in endoplasmic reticulum		Wnt signaling pathway		Apoptosis	
HSPA2	0.445	HSPA2	0.445	PRKX	0.709	PRKX	0.709
LDLRAP1	0.421	DDOST	0.421	PRKCG	0.581	NFKBIA	0.452
TGFB3	0.42	SSR4	0.454	FZD9	0.423	PIK3R5	0.619
TGFB1	0.384	SKP1	0.392	PLCB3	0.537	PRKACA	0.62
VPS25	0.342	MAPK8	0.56	TCF7L1	0.436	PRKACB	0.577
PRKCI	0.459	HSP90B1	0.374	PRKACA	0.62	PPP3R1	0.395
CDC42	0.547	DNAJC10	0.367	NFATC4	0.38	CASP9	0.366
ERBB3	0.411	UBE2D1	0.367	SKP1	0.392	AKT3	0.453
AP2B1	0.328	SEC31A	0.446	MAPK8	0.56	PPP3CB	0.37
CXCR4	0.337	SEC63	0.375	WNT10B	0.363	IKBKG	0.569
TSG101	0.453	HSP90AB1	0.339	PLCB1	0.491	PRKAR1A	0.276
RAB11A	0.384	SAR1A	0.36	PPP2R1A	0.38	IL1RAP	0.298
SMAD3	0.434	FBXO2	0.304	PRKACB	0.577	IRAK2	0.267
RAB5C	0.33	TUSC3	0.322	PPP3R1	0.395	TNFRSF10D	0.251
RAB11FIP2	0.325	MAPK10	0.517	NFATC2	0.321	CASP6	0.26
VTA1	0.334	DDIT3	0.368	PORCN	0.316	PIK3R1	0.511
CHMP5	0.314	SEC61B	0.381	SMAD3	0.434	PRKAR1B	0.237
PARD3	0.304	SSR2	0.345	MAPK10	0.517	PPP3CA	0.322
AP2M1	0.295	SEC61G	0.38	NLK	0.305	CYCS	0.319
VPS37A	0.291	UBQLN1	0.301	CAMK2D	0.336	IKBKB	0.34
CLTC	0.289	PLAA	0.312	CSNK2A1	0.293	CAPN2	0.242
ASAP1	0.276	EIF2S1	0.312	PPP3CB	0.37	PRKAR2B	0.216
PIP5K1A	0.35	STT3B	0.335	MAP3K7	0.374	CASP7	0.245
DNM1L	0.292	UBE2E3	0.308	PPP2CA	0.339	PIK3CB	0.468
RAB5A	0.339	CKAP4	0.465	PPP2R5C	0.282	RELA	0.395
ERBB4	0.521	GANAB	0.378	GSK3B	0.404	PPP3CC	0.279
CHMP2A	0.295	MAPK9	0.499	MAPK9	0.499	CASP10	0.191
CHMP4A	0.296	DNAJC5G	0.345	CTNNA1	0.685	TNFRSF10B	0.178
TRAF6	0.415	DNAJA2	0.345	TBL1XR1	0.275	AIFM1	0
AP2A2	0.27	DNAJC5	0.344	FZD8	0.307	BCL2	0.233
MET	0.404	SEC61A2	0.372	ROCK1	0.326	RIPK1	0.186
CHMP1B	0.384	UBE2E2	0.304	PPP2R5E	0.258	NFKB1	0.372
DNM3	0.272	VCP	0.368	WNT10A	0.27	DFFA	0.168
VPS36	0.262	ERP29	0.274	CAMK2A	0.295	BIRC3	0.192
CHMP2B	0.279	DERL3	0.297	BTRC	0.267	CAPN1	0.165
PDCD6IP	0.291	UGGT2	0	FZD7	0.271	APAF1	0.133
ZFYVE16	0.249	SVIP	0.317	PPP3CA	0.322	EXOG	0
EPS15	0.265	HYOU1	0.39	LRP5	0.241	BIRC2	0.173
ARAP1	0	6-Mar	0.324	RBX1	0.443	CASP3	0.236
CHMP4B	0.275	UBQLN2	0.271	CHD8	0.215	PIK3CD	0.404
CSF1R	0.372	DNAJB11	0.278	CSNK2A2	0.221	FAS	0.125
AP2A1	0.249	SEL1L	0.245	PPP2R5D	0.217	IRAK1	0.172
DNM1	0.252	UBE2E1	0.276	SFRP2	0.239	TRAF2	0.189
AP2S1	0.246	MBTPS2	0	RUVBL1	0.22	MYD88	0.185
STAM	0.259	ERLEC1	0	RAC1	0.616	XIAP	0.153
CAV1	0.234	SEC23A	0.26	PRICKLE1	0.218	TNFSF10	0.177
RAB5B	0.269	MAN1A2	0.259	PRKCB	0.372	MAP3K14	0.182
RAB11FIP4	0.263	DERL2	0.257	CUL1	0.239	IRAK4	0.159
PRKCZ	0.365	RAD23A	0.375	PPP2R5B	0.205	ENDOD1	0
SMAP2	0	CALR	0.263	CSNK1A1	0.207	AKT1	0.288
PSD4	0	RBX1	0.443	FRAT2	0.196	CASP8	0.157
EHD3	0.224	EIF2AK1	0.259	PPP2CB	0.248	TNFRSF1A	0.125
PSD2	0	NSFL1C	0.271	PPP3CC	0.279	IRAK3	0.0954
RAB7A	0.253	SEC13	0.351	CCND2	0.282	BCL2L1	0.1
EEA1	0.271	BCAP31	0.285	RAC3	0.506	TRADD	0.145

(Contd...)

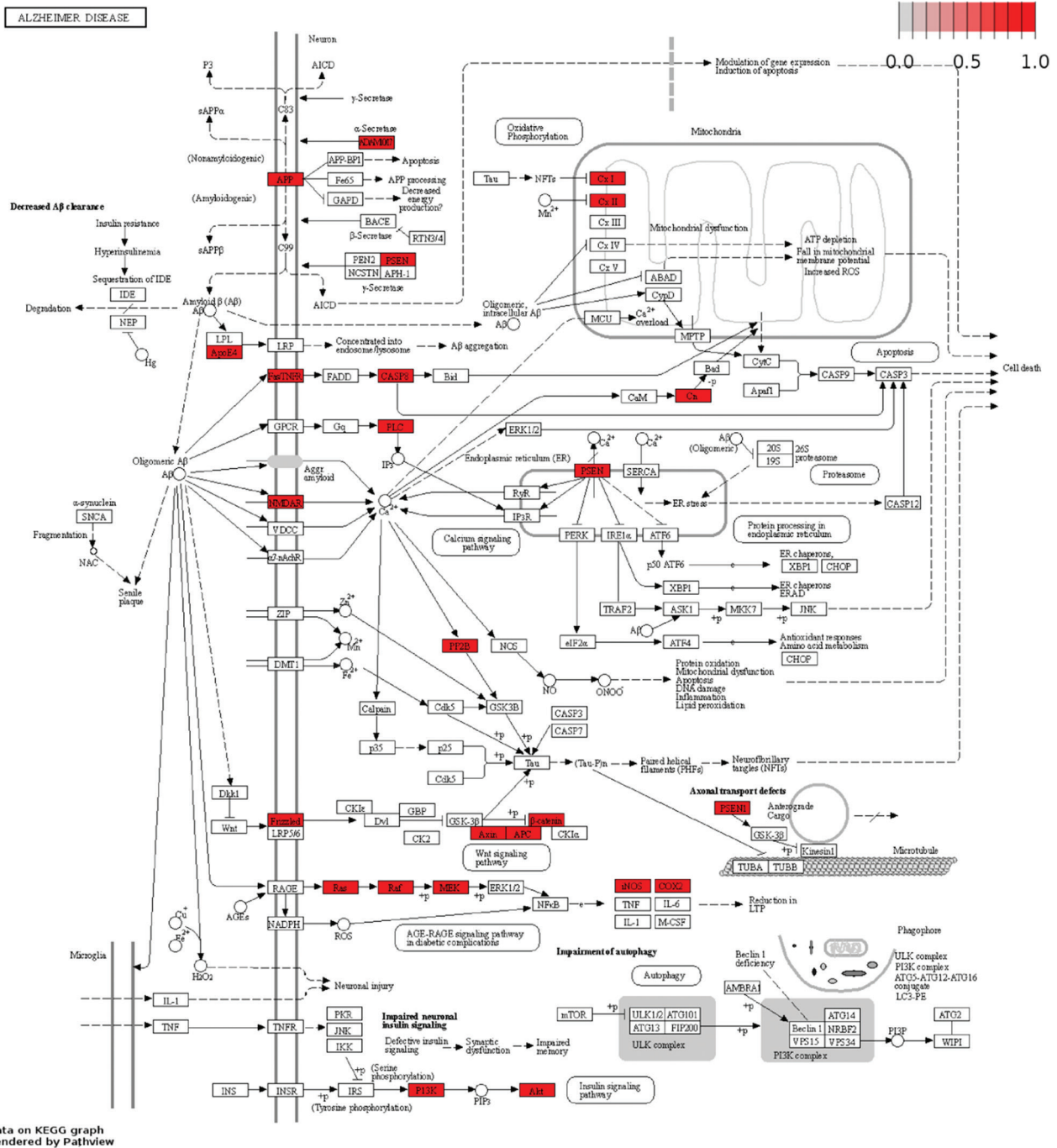
**SUPPLEMENTAL TABLE 5. (Continued)**

Endocytosis		Protein processing in endoplasmic reticulum		Wnt signaling pathway		Apoptosis	
KIT	0.334	HSPA8	0.258	CTNNBIP1	0.176	PRKAR2A	0.08
HSPA8	0.258	EDEM1	0	SOX17	0.186	BID	0.0755
SH3GL2	0.234	CAPN2	0.242	PLCB4	0.361	BAX	0.0914
AGAP2	0	RPN2	0.242	DAAM2	0.171	CFLAR	0.0684
PSD3	0	RAD23B	0.364	PPP2R1B	0.234	AKT2	0.25
NEDD4L	0.259	PDIA3	0	NFATC1	0.176	IL1R1	0.0976
HRAS	0.42	SSR1	0.281	TBL1X	0.166	PIK3CA	0.353
DNAJC6	0	MAP2K7	0.453	DAAM1	0.163	ENDOG	0
MDM2	0.25	SEC62	0.259	SFRP1	0.192	FADD	0.155
HGS	0.22	MAN1B1	0.237	CACYBP	0	BAD	0.127
PIP5K1B	0.283	SEC23B	0.235	DVL3	0.36	CHUK	0.132
CLTA	0.21	HSPBP1	0	NKD2	0.151	TP53	0.895
IQSEC2	0	CUL1	0.239	RHOA	0.438	ATM	0.0249
VPS45	0	UBXN6	0.251	FZD1	0.192	PIK3R3	0.329
SH3KBP1	0.213	HSPA4L	0	CCND3	0.252	DFFB	0.0197
FLT1	0.273	XBP1	0.21	WNT3	0.172	PRKX	0.709
SMURF1	0.223	UBE2D2	0.232	PRICKLE2	0.157	NFKBIA	0.452
ARFGAP2	0	DERL1	0.235	PRKCA	0.323	PIK3R5	0.619
RAB31	0	CANX	0	FZD3	0.189	PRKACA	0.62
VPS4B	0.268	RPN1	0.223	PPP2R5A	0.147	PRKACB	0.577
SRC	0.264	ATF6	0.216	LEF1	0.224	PPP3R1	0.395
CHMP6	0.188	DNAJC1	0.225	TCF7L2	0.223	CASP9	0.366
SH3GLB2	0.197	MOGS	0.4	WNT7A	0.162	AKT3	0.453
PSD	0	SEC31B	0.323	LRP6	0.148	PPP3CB	0.37
RNF41	0.194	MAN1A1	0.217	ROCK2	0.21	IKBKG	0.569
ARAP3	0	EDEM3	0	FRAT1	0.132	PRKAR1A	0.276
GIT2	0	UBE4B	0.208	AXIN1	0.244	IL1RAP	0.298
ZFYVE9	0.171	SSR3	0.255	NKD1	0.124	IRAK2	0.267
ARRB2	0.174	RRBP1	0	PPARD	0.198	TNFRSF10D	0.251
SMAD7	0.184	HSPA5	0.22	AXIN2	0.238	CASP6	0.26
RAB22A	0	UBE2D3	0.212	SEN2	0.117	PIK3R1	0.511
PIP5KL1	0.189	EDEM2	0	NFAT5	0.131	PRKAR1B	0.237
ITCH	0.177	BCL2	0.233	FBXW11	0.146	PPP3CA	0.322
EHD2	0	SEC24B	0.203	TCF7	0.198	CYCS	0.319
RAB11FIP1	0.196	LMAN2	0	CTBP1	0.132	IKBKB	0.34
ACAP2	0	LMAN1	0	VANGL2	0.117	CAPN2	0.242
RAB11B	0.249	HSPH1	0	SIAH1	0.0965	PRKAR2B	0.216
RHOA	0.438	P4HB	0.165	CSNK1E	0.147	CASP7	0.245
IQSEC1	0	STT3A	0.227	JUN	0.158	PIK3CB	0.468
RET	0.201	SEC24A	0.19	WNT5B	0.111	RELA	0.395
NEDD4	0.164	PREB	0.183	APC2	0.147	PPP3CC	0.279
RAB11FIP3	0.182	AMFR	0.22	FZD5	0.123	CASP10	0.191
STAM2	0.168	MBTPS1	0	WNT7B	0.0944	TNFRSF10B	0.178
ARFGAP1	0	DNAJB12	0.235	VANGL1	0.0865	AIFM1	0
PLD1	0.235	SIL1	0.297	FZD4	0.11	BCL2	0.233
SNF8	0.487	UBQLN4	0.174	SMAD2	0.229	RIPK1	0.186
CBLB	0.238	UBE2G1	0.174	DVL2	0.279	NFKB1	0.372
EPN1	0.146	SYVN1	0.236	CCND1	0.201	DFFA	0.168
HSPA1L	0.17	STUB1	0.183	CSNK2B	0.0591		
GIT1	0.141	PDIA6	0.153	WNT5A	0.0751		
GRK5	0.128	UBE2J2	0.17	APC	0.111		
SH3GL3	0.144	UBE2J1	0.167	CREBBP	0.167		
FGFR2	0.254	OS9	0	DVL1	0.262		
FOLR2	0	DNAJA1	0.226	SMAD4	0.17		
DNM2	0.142	CAPN1	0.165	CTBP2	0.0644		
SMAD6	0.143	PPP1R15A	0.149	MYC	0.212		
IQSEC3	0	RNF5	0.204	WNT2B	0.0626		
VPS28	0.133	CRYAB	0	PSEN1	0.0927		
STAMBP	0	MANIC1	0.166	CAMK2G	0.0927		
RUFY1	0.126	NGLY1	0.155	PLCB2	0.237		

(Contd...)

**SUPPLEMENTAL TABLE 5. (Continued)**

Endocytosis		Protein processing in endoplasmic reticulum		Wnt signaling pathway		Apoptosis	
GRK6	0.118	HSPA1L	0.17	CXXC4	0.0259		
RAB4A	0.166	DNAJB2	0.207	FZD6	0.0723	mTOR signaling pathway	
WWP1	0.133	EIF2AK4	0.16	CAMK2B	0.0775		
ADRB1	0.134	FBXO6	0.119	RAC2	0.404	PIK3R5	0.619
TFRC	0	UGGT1	0	TP53	0.895	DDIT4	0.363
RABEP1	0.183	SEC24C	0.149	WIF1	0.0292	RPS6KA1	0.34
PLD2	0.212	NPLOC4	0.138	NFATC3	0.0251	MAPK1	0.729
TGFB2	0.148	WFS1	0			PRKAA2	0.353
ACAP1	0	TRAF2	0.189	Type II diabetes mellitus		AKT3	0.453
EHD1	0.21	ATF6B	0.109			PGF	0.314
TGFBR2	0.146	SEC24D	0.138	PIK3R5	0.619	BRAF	0.355
RAB11FIP5	0.13	PRKCSH	0	MAPK8	0.56	RHEB	0.337
ARF6	0.217	ERN1	0.141	CACNA1D	0.396	RPS6KA6	0.282
ARRB1	0.0922	DAD1	0.124	MAPK1	0.729	EIF4E2	0.261
VPS37B	0.0939	HSP90AA1	0.122	MAPK10	0.517	PIK3R1	0.511
PDGFRA	0.249	BAK1	0.0861	ABCC8	0.295	ULK2	0.229
EHD4	0	EIF2AK3	0.125	HK1	0.476	STRADA	0
CLTB	0.0934	PDIA4	0.09	CACNA1E	0.365	TSC1	0.245
FGFR4	0.199	ATXN3	0	MAPK9	0.499	PDPK1	0.303
HSPA1A	0.121	HSPA1A	0.121	CACNA1B	0.336	EIF4EBP1	0.259
EGFR	0.296	EIF2AK2	0.114	CACNA1G	0.334	VEGFB	0.232
KDR	0.17	BAX	0.0914	PIK3R1	0.511	EIF4B	0.209
USP8	0	YOD1	0.158	IKBKB	0.34	PIK3CB	0.468
ASAP3	0.0689	SAR1B	0.132	SOCS4	0.28	MAPK3	0.658
SMAP1	0	BAG2	0	HK2	0.406	MTOR	0.367
HLA-A	0.084	NFE2L2	0.0926	INSR	0.245	EIF4E	0.197
ASAP2	0.0639	UBE2D4	0.101	PIK3CB	0.468	RPS6KA3	0.191
HLA-C	0.0801	MAP3K5	0.163	MAPK3	0.658	RPS6KB1	0.214
ARFGAP3	0	TRAM1	0.114	MTOR	0.367	CAB39	0
PARD6A	0.07	UBE2G2	0.0869	CACNA1C	0.278	RPTOR	0
ACAP3	0	HERPUD1	0.0481	CACNA1A	0.229	TSC2	0.315
SMAD2	0.229	HSPA1B	0.0827	PIK3CD	0.404	HIF1A	0.327
PARD6B	0.0661	DNAJB1	0.119	HK3	0.315	ULK1	0.121
HLA-E	0.0716	SEC61A1	0.152	KCNJ11	0.075	MLST8	0
CBL	0.168	DNAJC3	0.0571	SOCS3	0.145	RPS6KB2	0.173
PIP5K1C	0.144	ATF4	0.166	GCK	0.123	PIK3CD	0.404
GRK4	0.0525	BAG1	0	PIK3CA	0.353	PRKAA1	0.174
SH3GL1	0.0681			IRS1	0.114	CAB39L	0
PML	0.0582			SLC2A4	0.198	AKT1	0.288
LDLR	0.181			SOCS2	0.116	VEGFA	0.111
TGFBR1	0.0808			IRS2	0.079	RPS6KA2	0.101
SH3GLB1	0.062			PIK3R3	0.329	RPS6	0.0767
VPS37D	0.0502					AKT2	0.25
HSPA1B	0.0827					PIK3CA	0.353
VPS37C	0.0431					RICTOR	0
CLTCL1	0.045						
CAV2	0.0316						
HLA-F	0.0462						
VPS4A	0.127						
EPN2	0.0483						
ARAP2	0						
DAB2	0.0449						
EPN3	0.043						
IGF1R	0.219						
SMURF2	0.0547						
AGAP1	0						
HLA-B	0.0319						
FGFR3	0.137						



Data on KEGG graph  
Rendered by Pathview

**SUPPLEMENTAL FIGURE 1.** Genes associated with other diseases act to Alzheimer's disease pathway. The red rectangles represent biological processes involved in genes associated with other diseases.